Guideline for synthesis and surface chemistry characterization of 2D Mo/Ti solid solutions based MXene. Application to hydrogen evolution reaction in alkaline media

Lola Loupias, Cláudia Morais, Sophie Morisset, Christine Canaff, Zheming Li, Florian Brette, Patrick Chartier, Nadia Guignard, Laetitia Maziere, Vincent Mauchamp, et al.

Guideline for synthesis and surface chemistry characterization of 2D Mo/Ti solid solutions based MXene. Application to hydrogen evolution reaction in alkaline media.

Lola Loupias[a], Cláudia Morais[a], Sophie Morisset[a], Christine Canaff[a], Zheming Li[a], Florian Brette[b], Patrick Chartier[b], Nadia Guignard[a], Laetitia Maziere[a], Vincent Mauchamp[b], Thierry Cabioc'h[b], Aurélien Habrioux[a,*], Stéphane Célérier [a,*]

[a] Institut de Chimie des Milieux et Matériaux de Poitiers (IC2MP), Université de Poitiers, CNRS, F-86073 Poitiers, France

[b] Institut Pprime, UPR 3346 CNRS, Université de Poitiers, ISAE-ENSMA, BP 30179, 86962 Futuroscope-Chasseneuil Cedex, France

Corresponding authors:

aurelien.habrioux@univ-poitiers.fr, stephane.celerier@univ-poitiers.fr

Abstract:
2D MXenes have gained an ever-increasing attention in various application fields owing to the combination of their layered structure with their excellent physico–chemical properties. MXene properties can be strongly tuned by modifying the M element in the $M_{n+1}X_nT_x$ structure. Among them, Mo-based MXenes are beginning to be successfully explored in many areas. However, few studies dealt with the synthesis and characterization of the $(Mo,Ti)_{n+1}C_nT_x$ solid solutions. The aim is to understand their complex chemistry in terms of structure, microstructure and surface chemical composition and to compare them with those of mono-metallic Mo_2CT_x and $Ti_3C_2T_x$ MXenes as well as parent MAX phases. Then, the potential of these materials as HER (hydrogen evolution reaction) catalysts is determined in alkaline medium, never done so far, and their activity is correlated with their surface chemistry. It is particularly shown that $Mo_2Ti_2C_3T_x$ MXenes are a credible alternative to Mo_2CT_x MXenes since the surface properties of both MXenes are similar while their composition is quite different. Indeed, the $(Mo,Ti)_{n+1}C_nT_x$ MXenes require lower temperatures and shorter time for the synthesis than for Mo_2CT_x MXenes, a great advantage from an industrial point of view. Finally, this study aims at providing a roadmap to carry out the synthesis and characterization of $(Mo,Ti)_{n+1}C_nT_x$ MXenes.

Keywords:
MXene, $(Mo,Ti)_{n+1}C_nT_x$, surface chemistry, surface properties, hydrogen evolution reaction

1. Introduction

2D transition metal carbides, nitrides and carbonitrides, named MXenes, have gained an ever increasing attention for a large range of application fields since their first appearance in 2011 [1] owing to the combination of their 2D layered structure with their excellent physico–chemical properties such as high thermal and electronic conductivity, high Young modulus, tunable electronic band gap, optical transparency, hydrophilic surface among others [2]. This new class of 2D materials has the following chemical formula, $M_{n+1}X_nT_x$, and are composed of $M_{n+1}X_n$ lamellae with M being a transition metal (TM) such as Ti, Cr, V, Mo and/or Nb, X being carbon or nitrogen, n ranging mainly from 1 to 4 and T stemming for terminal groups grafted to their surface. MXenes are produced from the exfoliation of nanolamellar ceramics, the MAX phases, with $M_{n+1}AX_n$ as general formulae, a very large materials family where A is an element from group 13 or 14 (mainly Al or Si) [2–5]. T groups are thus grafted onto the surface of $M_{n+1}X_n$ MXenes sheets during the removal of the A element layers from the MAX phase precursor which can be achieved in different etching environments. Using commonly used acidic etching agents (*e. g.*, HF or LiF/HCl) [6], the T groups are typically =O, -OH, -F and/or –Cl. They play a major role on MXenes surface properties [7–10]. In addition to the tuning of the chemical nature of T groups, the MXene properties can also be modified in depth by varying the nature of X as well as M elements. However, the change of X from C to N leads to the formation of nitrides or carbonitrides that are less stable than their corresponding carbides and tightly controlling the nature and distribution of T groups remains a challenge with standard exfoliation processes. Thus, the modification of M remains the simplest solution to tune MXenes properties in a controlled way. Beyond mono-transition metal (TM) MXenes, double-TM solid solution [11,12], double-TM ordered [13], ordered metal divacancies [14], and high-entropy [15] MXenes have also been synthesized, allowing to reach more than 40 different MXenes [2–4]. Among them, $Ti_3C_2T_x$ is the most studied one but Mo-based MXenes appear as highly promising candidates in many areas: batteries [16], heterogeneous catalysis [17–21], hydrogen electrocatalysis [22–24], oxygen electrocatalysis [25], CO_2 adsorption [26], thermoelectric applications [27], photocatalysis [28,29] or CO_2 electroreduction [30].

Though numerous studies focused on the Mo_2CT_x MXene, first synthesized in 2015 [31] and certainly the second most studied MXene so far, few studies deal with the synthesis and characterization of the $(Mo,Ti)_{n+1}C_nT_x$ solid solutions [13,32–34] (**Figure 1**) despite promising electrocatalytic performances towards hydrogen evolution reaction (HER) in acidic media [35]. Moreover, the used synthesis routes do not systematically lead to the production of phase pure materials and the characterizations of their properties are often incomplete. From a broader perspective, in-depth characterization of Mo/Ti solid solutions offer a unique way to establish a correlation between the structural and surface properties of MXene.

Through this fundamental study, the first objective is to understand the complex chemistry of $(Mo,Ti)_{n+1}C_nT_x$ in terms of structure, microstructure and surface chemical composition. It will be done thanks to physico-chemical characterization techniques such as XRD, SEM, EDX, ICP-OES, XPS and Raman spectroscopy. The chemistry of $(Mo,Ti)_{n+1}C_nT_x$ MXenes will be compared to those of mono-metallic Mo_2CT_x and $Ti_3C_2T_x$ MXenes and their corresponding MAX phases. XPS is particularly discussed since it is one popular tool for MXene characterization, providing specific information on the electronic properties of the examined elements. Even if these MXenes have already been characterized by XPS in a complete study published by Halim *et al.* [33], the studied materials suffered from a low purity due to their relatively high oxidation degree. Thus, our work aims at completing the above-mentioned study to get insight concerning the surface chemistry of these materials. Another objective is to evaluate the ability of these materials as HER catalysts in alkaline medium, never done so far, and to correlate their activity with their surface chemistry. Finding effective non-noble metal-based catalysts for HER in alkaline medium is indeed one major stumbling block for the large-scale development of low-cost anion exchange membrane water electrolyzers. It is particularly shown that $(Mo,Ti)_{n+1}C_nT_x$ MXenes exhibit similar surface chemistries and properties than the mono-metallic Mo_2CT_x MXene

while their composition is quite different. Finally, this study aims at providing a roadmap to carry out the synthesis and characterization of pure phase $(Mo,Ti)_{n+1}C_nT_x$ MXenes.

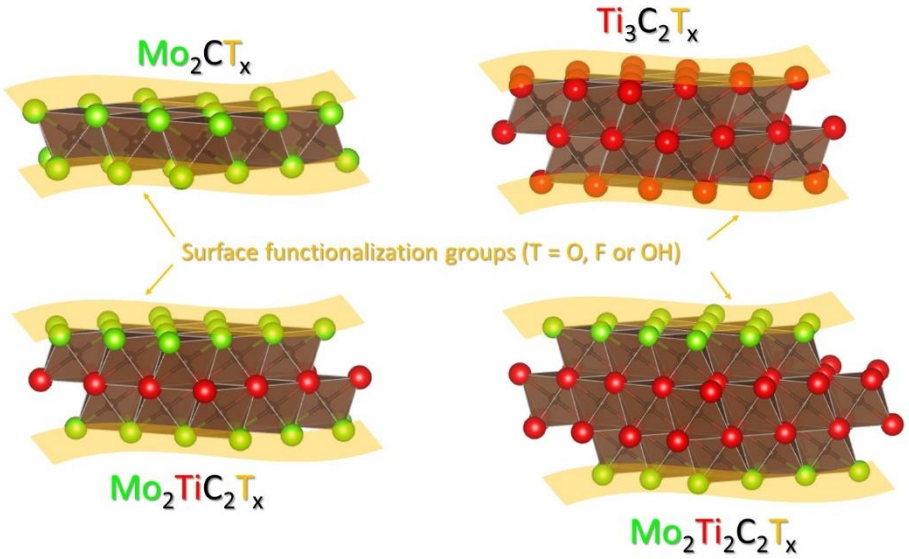

Figure 1. *Structures of the $(Mo,Ti)_{n+1}C_nT_x$ MXenes studied in this work.*

2. Experimental

2.1 Synthesis of materials

- MAX phases

Ti_3AlC_2 MAX phase powders were synthesized using a conventional powder metallurgy technique. Titanium (-200 mesh, 99.95%, Alfa Aesar Karlsruhe Germany), titanium carbide TiC (4 µm, 99.5%, Alfa Aesar) and aluminum (60-100 mesh 99.8%, Alfa Aesar) powders were used as starting materials. The powders were introduced in stoichiometric amounts (according to the Ti_3AlC_2 chemical formula) except for Al powder which was introduced with a 10 wt.% excess in order to compensate its loss by evaporation during the sintering process. After mixing for 30 min (Turbula Shaker Mixer), a homogeneous mixture without agglomerates is obtained. This mixture was packed into a glass tube sealed under vacuum. The sintering has been performed under argon atmosphere for 2 h at 1450 °C. Mo_2Ga_2C synthesis is based on the work of Halim *et al.* [36]. Briefly, gallium, Ga, with a melting point close to room temperature (RT), was added to a β-Mo_2C powder (~99.5% purity, Alfa Aesar, USA) in a 1:8 molar ratio. The mixture was thoroughly ground in a mortar and pestle until a homogenous paste-like mixture was obtained. The latter was then transferred into a quartz tube, which was placed under vacuum and was sealed off. The sintering has been performed at 850 °C for 168 h. After removing the resulting powder from the tube, it was soaked in 12 mol l^{-1} hydrochloric acid (HCl, TECHNICAL, VWR) while stirring at RT for 12 h to dissolve the excess of Ga. Lastly, the powders were centrifuged in ultrapure water several times at 4500 rpm until the pH of the solution was higher than 5, filtered and dried in air before further use. The other MAX phases, $Mo_2Ti_2AlC_3$ and Mo_2TiAlC_2, were purchased from Laizhou Kai Kai Ceramic Materials Co., based in China. Finally, the MAX powders were sieved to select grain sizes lower than 25 µm.

- MXenes

The syntheses of Mo_2CT_x, $Mo_2TiC_2T_x$ $Mo_2Ti_2C_3T_x$ and $Ti_3C_2T_x$ MXenes are partly based on the work of Halim *et al.* [33] using HF as etching agent. 0.5 g of the corresponding MAX phase precursor was

gradually added to 10 ml of hydrofluoric acid, HF, (50%—Sigma Aldrich) and heated at 60 °C for Mo_2CT_x, $Mo_2TiC_2T_x$ and $Mo_2Ti_2C_3T_x$ or 25 °C for $Ti_3C_2T_x$. The etching duration was of 196 h for Mo_2CT_x, 24 h for $Ti_3C_2T_x$, and 96 h (or 24 h) for $Mo_2TiC_2T_x$ and $Mo_2Ti_2C_3T_x$. The suspension obtained after etching was centrifuged several times at 3500 rpm (corresponding to 1575 g – rotor F-34-6-38, Eppendorf centrifuge 5804) for 2 min with ultrapure water until the pH of the supernatant was higher than 5. The supernatant was removed between each centrifugation.
To delaminate the multilayers, 5 ml of 1.5 mol L^{-1} aqueous tetrabutylammonium hydroxide, TBAOH, was added to the remaining slurry. The mixture was shaken for 1 min using a vortex and ultrasonicated for 30 min under Ar to promote intercalation of the TBA^+ ions. After sonication, absolute ethanol (≥ 99.9%, CARLO ERBA), EtOH, was added and the suspension was centrifuged at 3500 rpm (1575 g) for 2 min. The supernatant was removed and the procedure was repeated 4 times. Finally, ultrapure water was added and the mixture was centrifuged for 30 min at 2500 rpm (804 g). The supernatant and the sediment were filtered separately (unless mentioned). The filtrates were dried in a desiccator under atmospheric pressure and the obtained MXene film is placed into a tube and stored in a glove box under argon before further use.

2.2. Characterization of materials

XRD analysis of the MXene powders were carried out with a PANalytical EMPYREAN powder diffractometer using a CuKα radiation source ($K_{\alpha1}$ = 1.5406 Å and $K_{\alpha2}$ = 1.5444 Å). XRD patterns were collected between 3 and 70 ° with a 0.07° step and 420 s dwell time at each step (between 5 and 145 ° with a 0.026° step and 1200 s dwell time for Rietveld refinement of MAX phases). An ultra-fast X-Ray detector (X'Celerator) was used to collect the signals allowing an important decrease of analysis duration. Note that the MXene films, obtained after filtration, were characterized without grinding allowing to keep the preferential orientation when it is present.
The XPS analysis were carried out with a Kratos Axis Ultra DLD spectrometer using a monochromatic Al Kα source (1486.6 eV, 10 mA, 15 kV). Instrument base pressure was 9×10^{-8} Pa. High-resolution spectra were recorded using an analysis area of 300 µm × 700 µm and a 20 eV pass energy, corresponding to a Ag $3d_{5/2}$ Full width at Half Maximum (FWHM) of 0.55 eV. Data were acquired with 0.1 eV steps. All spectra presented in this work have their binding energy scale calibrated against the Fermi-edge. The strategy used for the curve fittings is discussed in the corresponding part of the manuscript.
Raman spectroscopy was carried out using a HORIBA Jobin Yvon LabRAM HR800 confocal Raman microscope with a CCD Peltier cooled detector. Spectra were acquired at RT using an excitation wavelength of 632.8 nm, supplied by an internal He-Ne laser. The power delivered at the sample is less than 1 mW. A 1800 grooves.mm^{-1} grating is used leading to a spectral resolution of 0.3 cm^{-1}. The results are collected using the Labspec 5 software. The spectrometer is calibrated by a silicon wafer.
Thermogravimetric analyses (TGA) were conducted with a Q600 SDT apparatus from TA Instruments coupled with a mass spectrometer (MS) (QGA-Hiden Analytical), using a heating rate of 10 °C min^{-1} from 20 to 400 °C under argon.
The Al, Ti, Mo, Ga contents of the different MAX and MXenes were determined by Inductively Coupled Plasma-Optical Emission Spectrometry (ICP-OES) using an Agilent 5110 VDV instrument.
The morphology of the samples was studied using a field emission gun scanning electron microscope (FEG-SEM) 7900F from JEOL. This microscope is equipped with an Energy Dispersive X-ray Spectrometer (EDS) from Bruker (with Esprit software) allowing the determination of the O, F, Al, Ti, Mo, Ga and C contents (semi-quantitative analyses).
Note here that all characterizations were performed on fresh samples (*i.e.* less than 24 h after the synthesis).

2.2. Electrochemical measurements

All electrochemical measurements were carried out at RT in a standard three-electrode electrochemical cell using a Biologic (SP-300) potentiostat coupled with a rotating disc electrode (RDE) on fresh samples. A commercial reversible hydrogen electrode (Hydroflex purchased by Gaskatel) and a glassy carbon plate were used, respectively, as reference and counter electrode. A 5 mm diameter glassy carbon (GC) disc was used as the working electrode substrate. The catalytic inks were prepared by dispersing 10 mg of catalyst powder in a mixture composed of ultra-pure water (500 µL), isopropanol (500 µL) and Nafion® (100 µL), followed by ultrasonication for 20 min. 7.5 µL of ink were deposited onto the surface of the working electrode (catalyst loading of 0.35 mg cm^{-2}) and the deposit was dried under N_2 flow. The measurements were conducted in a N_2 saturated 1 mol L^{-1} KOH (85%, VWR) aqueous electrolyte. Firstly, cyclic voltammograms were recorded in a nitrogen-saturated electrolyte from 0 to 0.35 V *vs.* RHE at a scan rate of 50 mV s^{-1}. Then the activity of catalysts towards HER was examined by recording linear sweep voltammograms from 0.2 to −0.5 V vs. RHE at a scan rate of 5 mV s^{-1} by applying a rotating rate of 1600 rpm to the working electrode. This is required to remove hydrogen bubbles from the electrode surface. Finally, a voltammetric cycle was recorded between 0.2 and 1.3 V vs. RHE to observe the irreversible oxidation peak associated to MXene surface oxidation. All measurements were IR-drop corrected by determining the cell resistance using electrochemical impedance spectroscopy measurements (EIS) between 0.1 Hz and 100 KHz.

3. Results and discussion

3.1 MAX phase synthesis and characterization

Having a good knowledge of the structure, composition and chemistry of the MAX phases is crucial to understand those of the corresponding MXenes. Indeed, previous works highlighted that the composition, the structural and physicochemical properties of the initial MAX phase (*e.g.*, grain size, crystallinity, purity) may vary as a function of the synthesis protocol and thus, affects the final properties of the corresponding MXene [37,38].

In this work, Ti_3AlC_2, $Mo_2Ti_2AlC_3$, Mo_2TiAlC_2 (MAX phases) and Mo_2Ga_2C (related MAX phase) were studied. Thus, a titanium content of 100, 50, 33 and 0% in the positions occupied by the M element in the corresponding MXenes is expected.

The X-Ray diffraction patterns recorded on the different MAX phases as well as their crystallographic structure are presented in **Figure 2**. For each one of them, the crystallographic structure was deduced from Rietveld refinements and the results are reported in **Figure S1-S4**. The Mo_2Ga_2C phase crystallizes in an hexagonal lattice ($P6_3/mmc$ space group) [39]. The same crystallographic structure is observed for Ti_3AlC_2 [40], Mo_2TiAlC_2 [41] and $Mo_2Ti_2AlC_3$ [42]. The lattice parameters obtained as result of the best refinement procedure are reported in **Table 1**. The obtained weighted reliability factors ("weighted profile R-factor") Rwp and agreement indices χ^2 (see **Figure S1-S4**) indicate that the assumed structural model for refinements is reliable. Secondary phases have been identified on the diffraction patterns of the MAX phases (Mo_2C and Mo_2GaC in the case of Mo_2Ga_2C; Al_2O_3 for Ti_3AlC_2 and TiC for $Mo_2Ti_2AlC_3$ and Mo_2TiAlC_2). Considering that all the secondary phases are crystallized, an excellent purity (determined by refinement), greater than 97 wt.%, is obtained for each of these powders, thus validating the implemented synthesis protocols in this work and those used to produce commercial powders (**Table 1**). Hence, they will serve as a solid base for obtaining the corresponding MXenes.

Furthermore, Rietveld refinements allowed determining the Mo:Ti ratio in $Mo_2Ti_2AlC_3$ and Mo_2TiAlC_2 MAX phases thanks to the estimation of the occupancy rate of Mo and Ti atoms in the 4e and 4f Wyckoff positions for $Mo_2Ti_2AlC_3$ and the 2a and 4f Wyckoff positions for Mo_2TiAlC_2. Nevertheless, the uncertainty on this parameter can be rather high (because of the anisotropic grain shape or the presence of preferential orientation). In $Mo_2Ti_2AlC_3$, the refinement indicates that the 4f Wyckoff positions (ideally occupied by Ti) is occupied at 84% by Ti and 16% by Mo while the 4e Wyckoff positions (ideally occupied by Mo) is occupied at 79% by Mo and 21% by Ti. In a similar way, for Mo_2TiAlC_2 MAX phase, the 2a Wyckoff positions (theoretically occupied by Ti) is 88% occupied by Ti

and 12% by Mo while the 4f Wyckoff positions (theoretically occupied by Mo) is 89% occupied by Mo and 11% by Ti. This result indicates that the "ideal" structure [42] is not completely obtained and that the Mo layer contains a fraction of Ti atoms. Anasori *et al*. observed the same trend, finding 25 % and 23% of Ti occuping Mo site in Mo_2TiAlC_2 and $Mo_2Ti_2AlC_3$, respectively [42]. In the ideal structure the surface layer is only composed of Mo atoms, the presence of 10-20% of Ti atoms in this layer may thus have a major impact on the surface properties of the corresponding MXenes.

Table 1: *Summary of data obtained from structure refinements using the Rietveld analysis for the different MAX phases investigated here.*

MAX phase	a = b (Å)	c (Å)	Purity (%)*
Mo_2Ga_2C	3.035681(7)	18.08851(6)	97.3(2)
Mo_2TiAlC_2	2.99678(2)	18.6571(2)	97.9(1)
$Mo_2Ti_2AlC_3$	3.02068(3)	23.5461(2)	98.9(1)
Ti_3AlC_2	3.07285(3)	18.5524(3)	98.8(2)

* determined from Rietveld refinement

The morphology of the different MAX phases was examined by SEM (**Figure S5**). These materials consist of grains or aggregates with a size of several microns (all of them were sieved to have grains size lower than 25 μm). For the aluminum-based MAX phases (namely Ti_3AlC_2, $Mo_2Ti_2AlC_3$ and Mo_2TiAlC_2), the sheet structure of these three-dimensional nanolamellar ceramics can be observed. This characteristic is also found for Mo_2Ga_2C, but the grains, generally exhibiting a smaller size, have a “tile” shape [36,39].

To get insight on the materials composition, analyses were performed by ICP-OES. This technique allows estimating the Mo, Ti, Al and Ga contents (**Table 2**) but not the carbon content. The obtained contents are close to the expected values although a slight under-stoichiometry in Ga and a slight over-stoichiometry in Ti and Al are observed for Mo_2Ga_2C and for the Ti containing MAX phases, respectively. For $Mo_2Ti_2AlC_3$, a slight excess of Ti over Mo is observed. This result agrees with those obtained from Rietveld refinements that showed a Ti/Mo ratio of 1.1 (**Figure S4**). These different studies carried out by XRD, microscopy and chemical analyses make it possible to confirm that the expected MAX phases were obtained.

Table 2: *Summary of element content determined by ICP-OES for the MAX phases (uncertainty on the last number in brackets).*

MAX phase	Atom %				Chemical formula after normalization for 2 Mo or 3 Ti
	Mo	***Ti***	***Ga***	***Al***	
Mo_2Ga_2C	57.6(4)	-	39.7(3)	-	**$Mo_2Ga_{1.90}$**
Mo_2TiAlC_2	63.6(8)	16.4(8)	-	10.4(9)	**$Mo_2Ti_{1.03}Al_{1.16}$**
$Mo_2Ti_2AlC_3$	51.9(7)	27.3(9)	-	9.7(8)	**$Mo_2Ti_{2.10}Al_{1.33}$**
Ti_3AlC_2	-	70.9(4)	-	15.0(3)	**$Ti_3Al_{1.13}$**

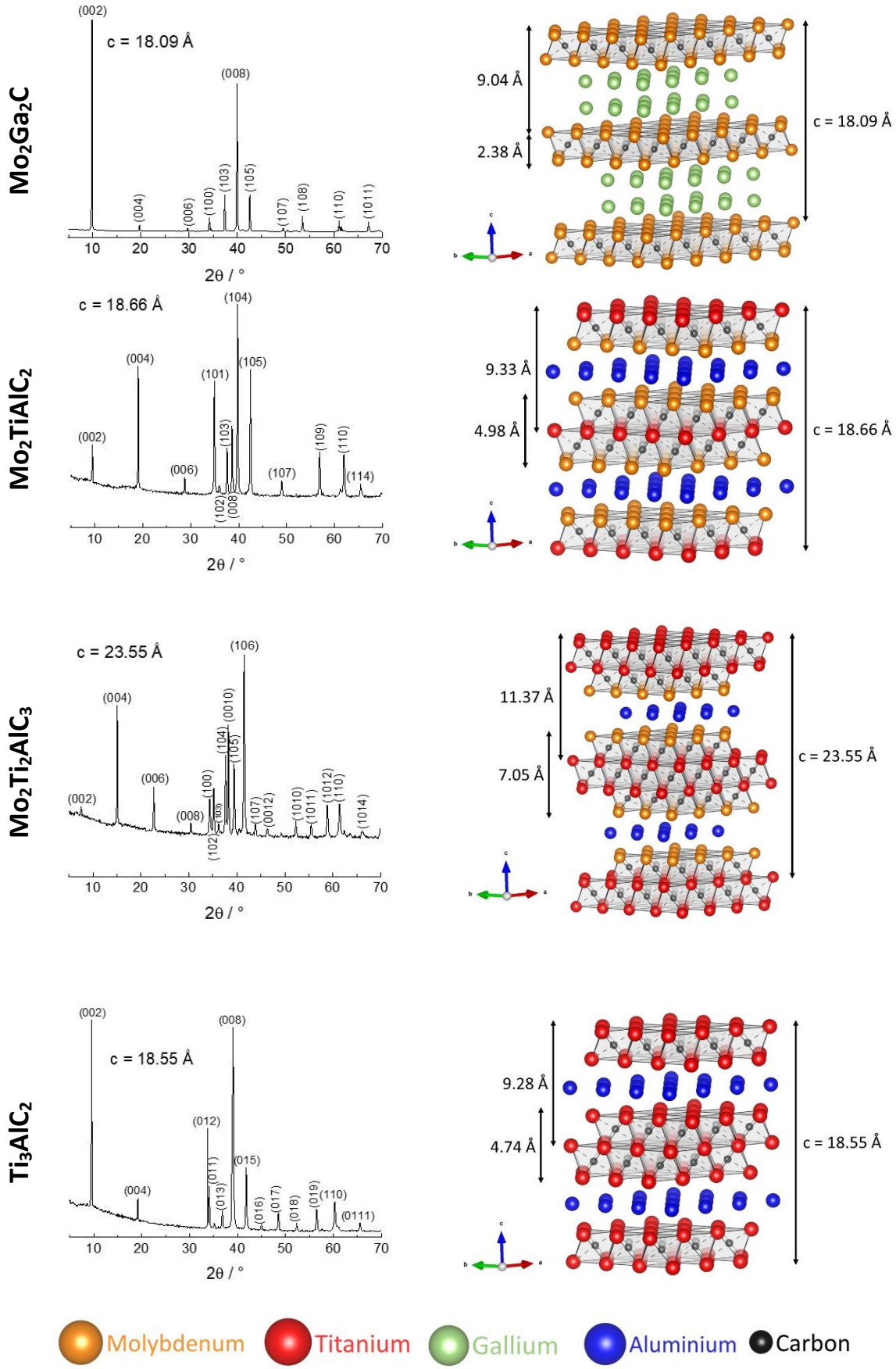

Figure 2. *X-Ray diffraction patterns and crystallographic structure representations of MAX phases.*

3.2 MXenes synthesis and characterization

Protocols based on the same etching and delamination agents were chosen in order to minimize the differences between the obtained MXenes (state of delamination, rate of exfoliation, terminal groups…) and thus to be able to compare their electrochemical performances afterwards. The HF etching agent was chosen rather than softer agents such as LiF/HCl because it is the most efficient one to etch Mo_2Ga_2C phase. Given the significant difference in reactivity of the studied MAX phases (different nature of A element, variation in bond strengths), the duration and temperature of the etching process has to be adjusted.

Synthesis of Mo_2CT_x and $Ti_3C_2T_x$

Several MAX phases, such as Mo_2AlC, Mo_2GaC and Mo_2Ga_2C, can potentially be used as precursor for the synthesis of Mo_2CT_x MXene [31,43,44]. Of these, only Mo_2Ga_2C has been shown to yield the Mo_2CT_x MXene [31,45]. However, this phase is the most refractory to exfoliation among the different MAX phases studied in this work due to the stronger Ga-Mo bond in comparison with the Al-Mo and Al-Ti bonds encountered in the other MAX phases [46]. To obtain pure MXene, it is therefore necessary to perform several steps: 1) immersion of Mo_2Ga_2C in 48% HF for 7 days at 60 °C, 2) washing with water by centrifugation; 3) immersion in aqueous tetrabutylammonium hydroxide $(C_4H_9)_4NOH$ (named TBAOH) solution under ultrasonication; 4) washing by centrifugation with water and recovery of the supernatant for 5) filtration and drying at ambient temperature. The synthesis is schematically represented in **Figure 3** and fully detailed in the experimental part.

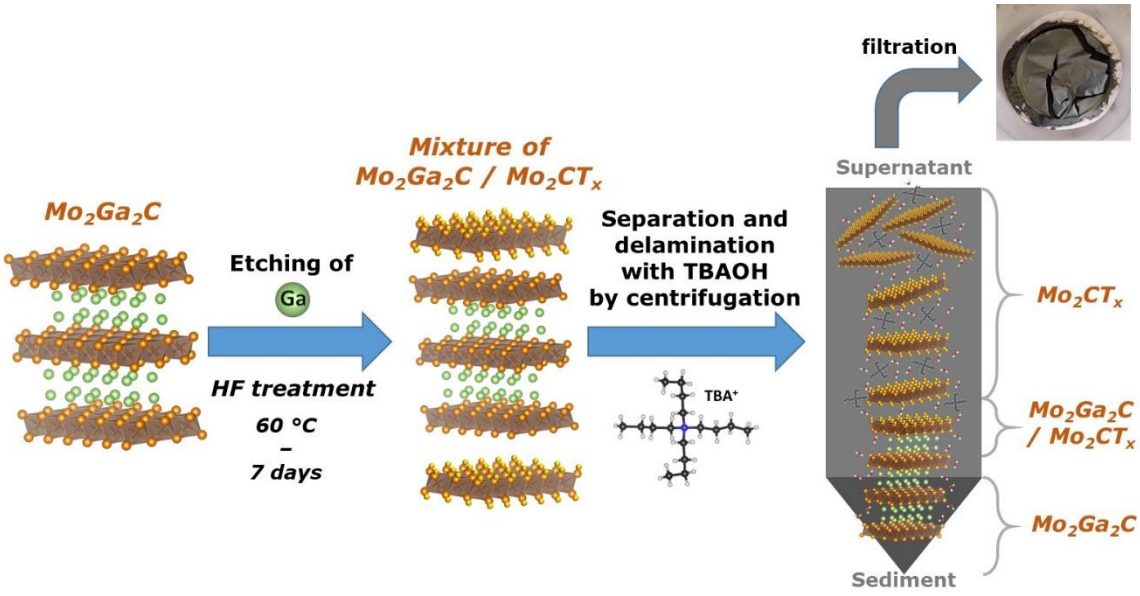

Figure 3. *Schematic representation of Mo_2CT_x synthesis.*

As the MAX phase is rather difficult to etch entirely, the insertion of TBAOH (or more precisely $(C_4H_9)_4N^+$ ions labelled TBA^+ and stabilized by water molecules) between the MXene sheets to perform delamination is required in order to separate the MXene from the unreacted MAX phase. The diffractograms of the filtrated and dried supernatant and sediment after centrifugation are reported in **Figure 4**. MXene formation is confirmed by the presence of the (002) peak at the low angles leading to a *c* lattice parameter of 25.30 Å. The (002) peak is strongly shifted towards lower angles (in comparison with diffraction pattern recorded with the MAX phase), indicating an increase of the *c* lattice parameter (18.09 Å for the MAX phase). This phenomenon results from the formation of terminal groups and the insertion of TBA^+ ions between the sheets [36]. Contrarily to the dried

sediment, no trace of the initial MAX phase is observed in the dried supernatant, confirming that the MXene/unreacted MAX phase separation by delamination with TBAOH is effective.

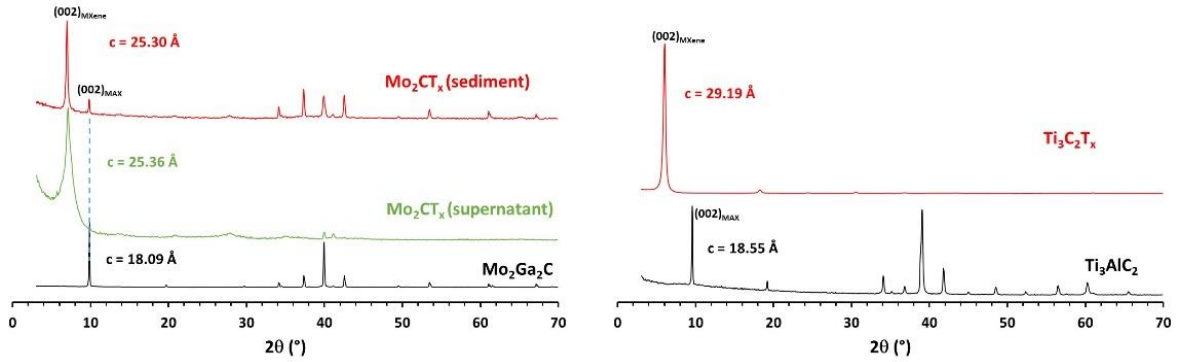

Figure 4. *XRD patterns of (left) Mo_2CT_x (sediment and supernatant) and (right) $Ti_3C_2T_x$ obtained after etching of Mo_2Ga_2C (left) and Ti_3AlC_2 (right) respectively. For comparison, the XRD of the corresponding MAX phase precursor are also given at the bottom of each graph. Diffractograms were vertically shifted for the sake of clarity.*

Though the Ti_3AlC_2 MAX phase can be fully exfoliated in 48% HF without requiring a separation step by delamination [6], the same protocol as that used for Mo_2Ga_2C was carried out. The aim is to avoid differences that could result from the exposition of $Ti_3C_2T_x$ MXene to other reagents and solvents. However, the time and temperature were greatly reduced (25 °C and 24 h instead of 60 °C and 168 h), the exfoliation step being much faster due to the higher reactivity of Ti-Al bond. Moreover, the supernatant and the sediment were not separated from each other since both of them only contain MXene, as confirmed by XRD (**Figure 4**). As expected, the c lattice parameter is higher (29.19 Å) than for a MXene synthesized using only 48% HF as etching medium without the insertion of TBA^+ ions (c = 19.90 Å) [6,47], this is due to the combined insertion of TBA^+ ions and water.

Synthesis of $Mo_2TiC_2T_x$ and $Mo_2Ti_2C_3T_x$

For the $Mo_2TiC_2T_x$ and $Mo_2Ti_2C_3T_x$ MXenes syntheses, the same protocol as that used for $Ti_3C_2T_x$ synthesis was carried out. The precursor powder was immersed in 48% HF during 24 h at 25 °C. This exfoliation step was followed by a delamination step thanks to TBAOH insertion. The diffractograms presented in **Figure S6** show that the etching of Al is not complete since the structural signature of the MAX phase is observed in the sediment. The MAX phase signature is even observed in the supernatant solutions recovered during $Mo_2TiC_2T_x$ synthesis, indicating that the MAX/MXene separation thanks to TBAOH insertion is not as effective as for Mo_2CT_x synthesis. However, the insertion of TBA^+ and water layers between the sheets is confirmed by the evolution of c lattice parameters that are of 34.61 Å and 37.33 Å for $Mo_2TiC_2T_x$ and $Mo_2Ti_2C_3T_x$, respectively. These values are higher than those calculated for the corresponding MAX phases that are of 18.66 Å and 23.55 Å for Mo_2TiAlC_2 and $Mo_2Ti_2AlC_3$, respectively.

In order to increase the exfoliation yield and recover pure MXene, the duration of the exfoliation step has been increased from 24 h to 96 h (**Figure 5**). Upon 96 h the MAX phase is almost never observed (only as a trace on the $Mo_2TiC_2T_x$ sediment pattern) both in the dried sediment and supernatant. The exfoliation is therefore total and the samples obtained after filtration of the sediment and the supernatant can be brought together. This last method was selected for the preparation of the MXenes studied in this work.

As observed on the XRD patterns presented in **Figure 5 and S6**, it is common to get *c* parameter variations of about 1 to 5 Å and different full width at half maximum (FWHM) even for identical

protocols. This is explained by the interstratification phenomenon leading to multiple interlayer spacings [48].

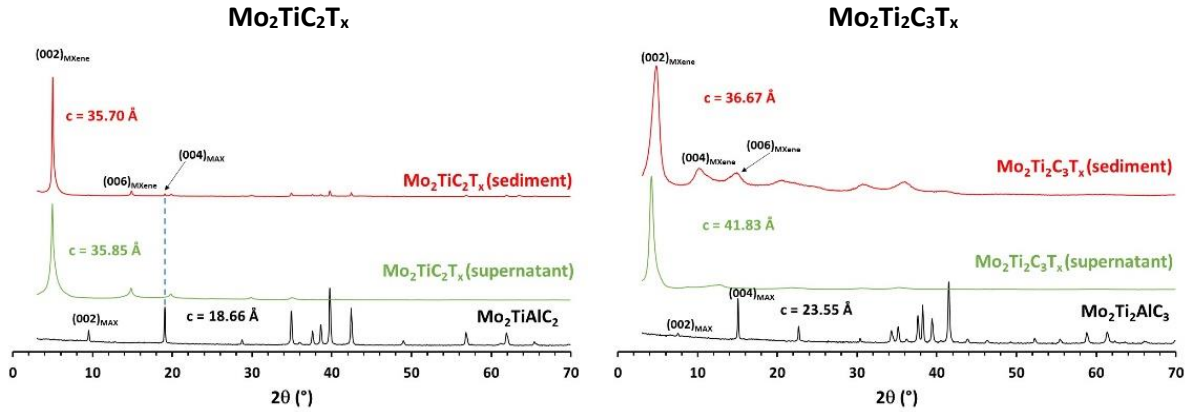

Figure 5. *XRD patterns of the sediments and supernatants of $Mo_2TiC_2T_x$ (left) and $Mo_2Ti_2C_3T_x$ (right) after etching of Mo_2TiAlC_2 and $Mo_2Ti_2AlC_3$ for 96 h. For comparison, the XRD of the corresponding MAX phase precursor are also given at the bottom of each graph. Diffractograms were vertically shifted for the sake of clarity.*

Structural and macrostructural properties of the MXenes

The *c* lattice parameters of the studied MXenes and of the corresponding MAX phases are reported in **Table 3**. As expected, the *c* parameter increases with the thickness of the $M_{n+1}X_n$ sheet, also reported in **Table 3** and deduced from **Figure 2**. From these data, the interlayer spacing (including terminal groups and inserted species (TBA^+ ions, water) can be estimated by the following equation**:**

Interlayer spacing = (c_{MXene} – 2 x thickness of the $M_{n+1}X_n$ sheet)/2 (eq. 1)

The obtained values are reported in **Table 3**. Even though, the uncertainty of this measurement is quite large due to the difficulty to determine precisely the average value of the *c* lattice parameter because of the interstratification phenomenon [48], it turns out that the interlayer spacing is relatively close for all MXenes (around 10 -13 Å), indicating that the nature of the inserted species is probably the same (water layer, TBA^+ ions).

Table 3: *c parameters calculated for MAX phases and MXenes, $M_{n+1}X_n$ sheet thickness and MXene interlayer spacing.*

c lattice parameter (Å)				$M_{n+1}X_n$ sheet thickness (Å)	Interlayer spacing including terminal groups (Å)
MAX phase*		**MXene**			
Mo_2Ga_2C	18.09	**Mo_2CT_x**	25.36	2.38	10.30
Mo_2TiAlC_2	18.66	**$Mo_2TiC_2T_x$**	35.70	4.98	12.87
$Mo_2Ti_2AlC_3$	23.55	**$Mo_2Ti_2C_3T_x$**	36.67	7.05	11.28
Ti_3AlC_2	18.55	**$Ti_3C_2T_x$**	29.19	4.74	9.86

* determined from Rietveld refinement

As for the common LiF/HCl route [6], the insertion of TBA^+ ions and H_2O molecules favors the delamination of the sheets, as confirmed from a macroscopic point of view. Indeed, the formation of films is observed after filtration and drying of MXenes (**Figure S7**), characteristic of delaminated sheets which are re-stacked after filtration. However, a “metallic” brightness is observed on molybdenum-based MXenes while this is not the case for $Ti_3C_2T_x$, suggesting a different reflecting power. In addition,

the latter is easily ground into a powder unlike Mo-based MXenes or $Ti_3C_2T_x$ prepared by the LiF/HCl route [6], indicating that the delamination is only partial for this sample despite the insertion of water and TBA^+ between the sheets. This result will be confirmed below.

Nature of inserted species between the MXenes sheets

To characterize the chemical nature of the inserted species, the syntheses of the MXenes were also performed without the delamination step in TBAOH (except for Mo_2CT_x for which this step is required to obtain pure MXene). As an example, **Figure 6a** shows the diffractograms recorded on $Mo_2TiC_2T_x$ sample obtained with and without (sample labelled $Mo_2TiC_2T_x$-nd) the delamination step. The XRD patterns were recorded on the different samples without grinding, to retain the preferential orientation when a film is obtained. As observed, the *c* lattice parameter is strongly impacted by the delamination step carried out in TBAOH with an increase of about 10 Å as a result of the insertion of TBA^+ ions (diameter close to 9.9 Å) [32] and water molecules. This evolution is also observed for $Mo_2TiC_2T_x$ and $Ti_3C_2T_x$ (**Figure S8-9**). The delamination is also confirmed by the disappearance of the (110) peak on **Figure 6b** for $Mo_2TiC_2T_x$ whereas it is clearly observed on $Mo_2TiC_2T_x$-nd, indicating a preferential orientation due to the formation of a film. This is furthermore confirmed by the SEM pictures (**Figure 6c).** The characteristic macrostructure of delaminated and restacked sheets is indeed observed for $Mo_2TiC_2T_x$ whereas the $Mo_2TiC_2T_x$-nd sample has more compact type multilayers microstructure (**Figure 6d)**, reflecting the lack of delamination. However, for $Ti_3C_2T_x$, the (110) peak is observed with or without the delamination step (**Figure S9)** indicating that delamination is not optimal for this MXene as discussed previously. This is also confirmed by SEM pictures with the same "accordion-like" multilayers microstructure for both $Ti_3C_2T_x$ samples (**Figure S9)**.

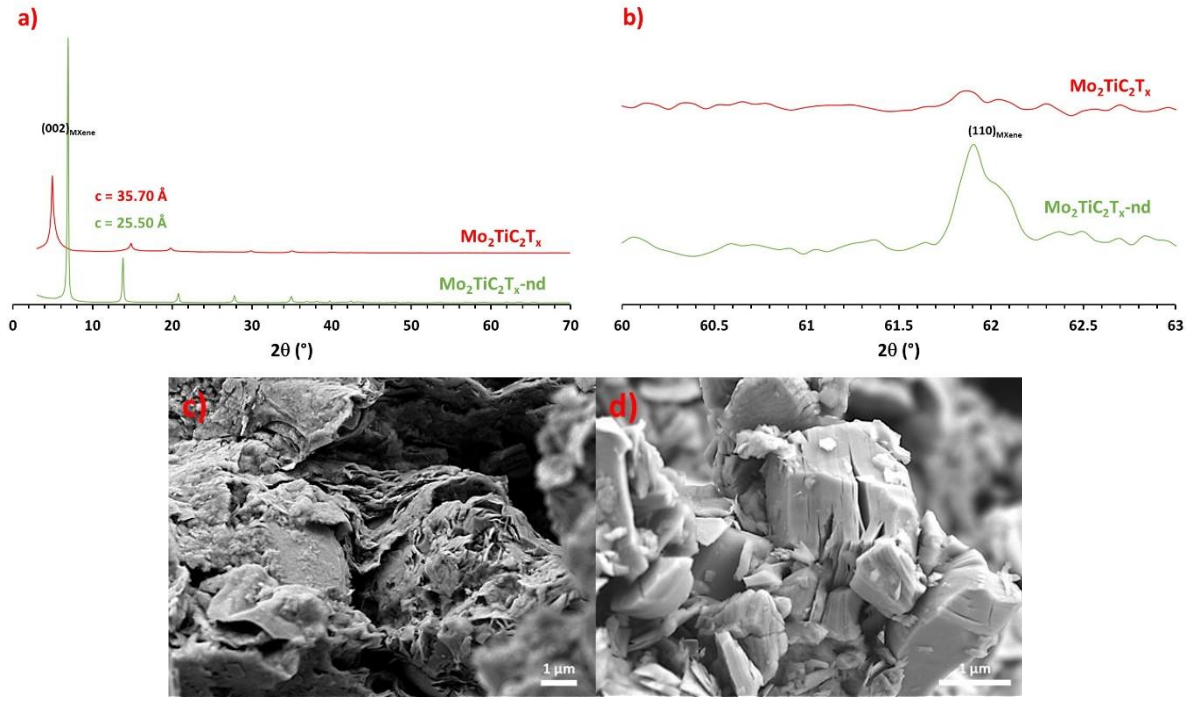

Figure 6. *a) XRD patterns of $Mo_2TiC_2T_x$ prepared with TBAOH step (red) and without (labelled $Mo_2TiC_2T_x$ – nd) (green). b) Magnification of the XRD patterns in 60-63 ° region to highlight the (110) peaks. SEM pictures of c) $Mo_2TiC_2T_x$ and d) $Mo_2TiC_2T_x$–nd.*

Thermogravimetric analyzes (TGA) coupled with a mass spectrometer (MS) were carried out under argon on the $Mo_2TiC_2T_x$-nd and $Mo_2TiC_2T_x$ samples (**Figure 7**). The most representative m/z ratios (mass to charge ratio) have been plotted in **Figure 7**. For both samples, a first mass loss is observed below 200 °C. This was attributed to a loss of water molecules (m/z = 18) that are either adsorbed on the MXene surface or inserted between the MXene sheets. This loss is higher in the case of the $Mo_2TiC_2T_x$ sample in comparison with $Mo_2TiC_2T_x$-nd (2.5% and 1.7% respectively). It is mostly probable that a larger amount of water molecules is intercalated in reason of the presence of TBA^+ ions.
Between 200 °C and 400 °C, a significant mass loss is observed only for $Mo_2TiC_2T_x$, corresponding to a loss of water (m/z = 18), CO_2 (m/z = 44) and mainly $CH_3CH_2^+$ (m/z = 29), associated to the decomposition of the TBA^+. At 400 °C, the global mass loss is significantly higher for $Mo_2TiC_2T_x$ than for $Mo_2TiC_2T_x$-nd samples. It is respectively of 8% and 2%. These analyses confirm the insertion of TBA^+ ions and water molecules between the sheets during the delamination step in the presence of TBAOH.

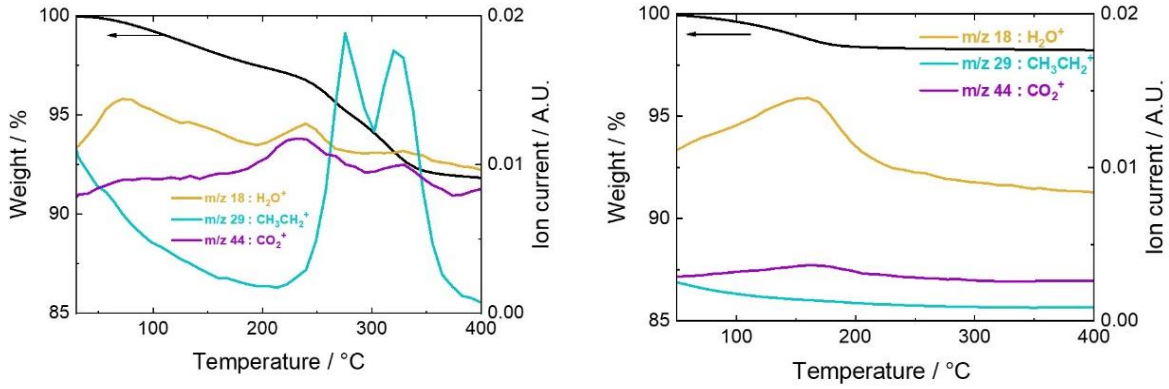

***Figure 7**. Thermal analyses performed under argon and coupled to mass spectrometry (TGA-MS) for $Mo_2TiC_2T_x$ prepared following to the delamination step (performed in the presence of TBAOH) (left) and for $Mo_2TiC_2T_x$ – nd prepared without immersion in TBAOH (right).*

Microstructural and chemical analyses of MXenes

The SEM pictures obtained for the four studied MXenes are reported in **Figure 8**. A typical microstructure of film is observed for the Mo containing samples (the sheets are clearly observed when the films are viewed edge-on), confirming the delamination, whereas the characteristic morphology of non-delaminated MXenes [6] is observed for $Ti_3C_2T_x$, confirming the macroscopic observations of the samples carried out after filtration and discussed previously. As above-mentioned the surface of $Ti_3C_2T_x$ only contains Ti atoms whereas the surface of the other MXenes mainly contains Mo atoms. Thus, the affinity of TBA^+ for surfaces consisting of closed packed Ti atoms is probably stronger than for Mo-containing surfaces, explaining the difficulty we face to delaminate $Ti_3C_2T_x$ sheets. Consequently, the LiF/HCl route [6,49,50] or the insertion of other organic solvents such as DMSO [51] is more suitable to promote the delamination of $Ti_3C_2T_x$.

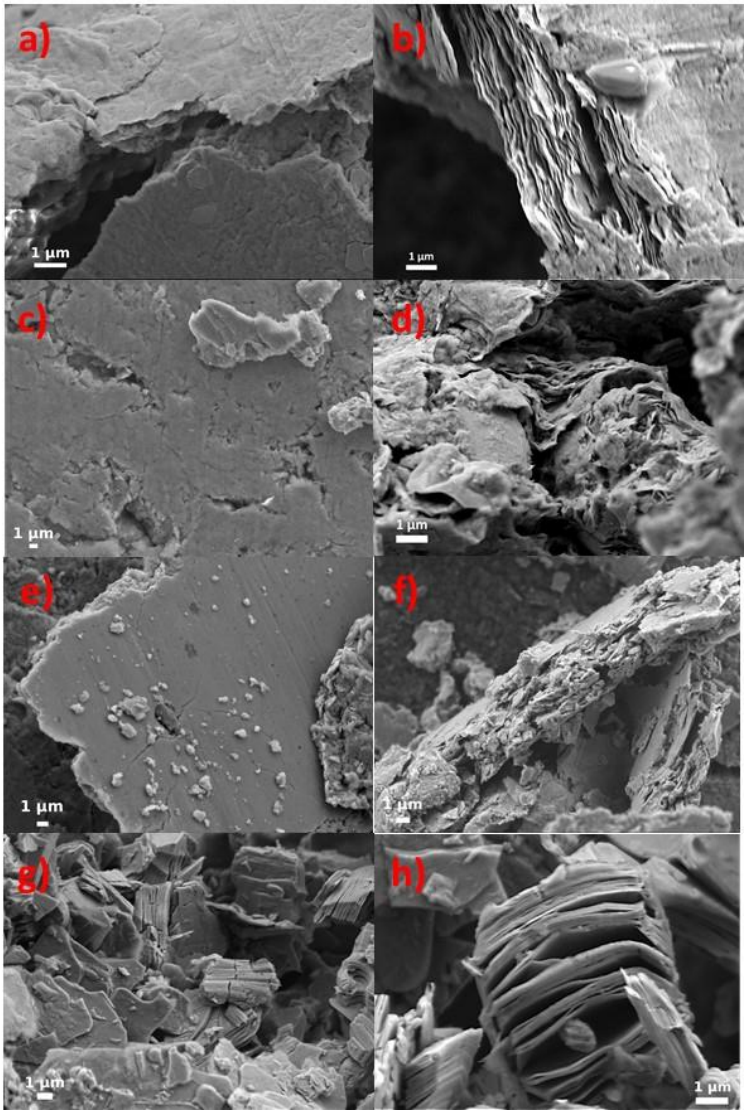

***Figure 8**. SEM pictures of a-b) Mo_2CT_x, c-d) $Mo_2TiC_2T_x$, e-f) $Mo_2Ti_2C_3T_x$ and g-h) $Ti_3C_2T_x$.*

The element contents determined by EDX are summarized in **Table 4.** For the solid solution phases, the initial Mo/Ti ratios determined for MAX phases are preserved during MXene synthesis, indicating that no significant dissolution of M element occurs during the exfoliation step. The A element (Ga or Al) is practically completely removed, confirming that the selected synthesis protocols are well suited to get MXenes without residual MAX phases. However, the carbon content is quite far from the expected value. This can be explained by the potential contribution of the carbon support used for SEM analysis but also due to the presence of carbon containing species such as TBA^+. Though contents of light elements such as fluorine and oxygen should be taken with caution, $Ti_3C_2T_x$ MXene has considerably more fluorine and less oxygen atoms than Mo containing samples, indicating the higher affinity of Ti for F terminal groups. ICP-OES analyses confirm the EDX analyses (**Table 5**), that is to know the removal of A element and the conservation of the Ti/Mo atomic ratio of the initial MAX phases even if a slight decrease (less than 10%) of the Ti content (see **Table 2** for comparison) cannot be excluded.

Table 4: *Summary of element content determined by EDS for the MXenes.*

MXene	Atom %								Chemical formula after normalization for 2 Mo or 3 Ti atoms
	Mo	***Ti***	***Ga***	***Al***	***C***	***O***	***F***	***Other elements***	
Mo_2CT_x	28	-	<0.5	-	31	36	2	4	$Mo_2C_{2.22}$
$Mo_2TiC_2T_x$	28	14	-	<0.5	31	24	2	1	$Mo_2Ti_{1.01}C_{3.21}$
$Mo_2Ti_2C_3T_x$	15	16	-	<0.5	38	28	2	1	$Mo_2Ti_{2.10}C_{3.28}$
$Ti_3C_2T_x$	-	31	-	<0.5	42	10	16	0	$Ti_3C_{4.04}$

Table 5: *Summary of element content determined by ICP-OES for the MXenes (uncertainty on the last number in brackets).*

MXene	Atom %				Chemical formula after normalization for 2 Mo or 3 Ti atoms
	Mo	***Ti***	***Ga***	***Al***	
Mo_2CT_x	70.8(5)	-	0.8(9)	-	$Mo_2Ga_{0.03}$
$Mo_2TiC_2T_x$	59.0(6)	13.4(2)	-	0.7(8)	$Mo_2Ti_{0.91}Al_{0.09}$
$Mo_2Ti_2C_3T_x$	35.6(9)	17.4(5)	-	0.4(9)	$Mo_2Ti_{1.96}Al_{0.07}$
$Ti_3C_2T_x$	-	60.1(1)	-	0.1(6)	$Ti_3Al_{0.01}$

Raman spectroscopy characterization of MXenes

The different materials were characterized by Raman spectroscopy which has been shown to provide valuable information about the bonding at the sheet level and the chemical nature of the T terminal groups [52]. The Raman spectra recorded with the MXenes and the corresponding MAX phases are plotted in **Figure 9**. In general, for the MAX phases, two distinct regions can be identified. The first one, between 100 cm^{-1} and 450 cm^{-1}, mainly corresponds to the vibrational modes related to the displacement of the metal M (Ti, Mo) and/or the element A (Al, Ga). The second one, between 550 cm^{-1} and 750 cm^{-1}, is ascribed to the vibrational modes related to the displacement of carbon atoms [53–56]. It turns out that for Mo_2Ga_2C (**Figure 9a**) no vibrational mode involving carbon atoms is active in Raman spectroscopy and consequently no band is observed in the 550-750 cm^{-1} region. The observed vibrational modes as well as their assignment are summarized in **Table S1**, for the four MAX phases studied herein.

The bands related to vibrations mainly involving the A element should be strongly affected by comparing the MXenes and the corresponding MAX phases. Furthermore, during exfoliation, terminal groups are grafted onto the MXene sheet surface, which might create shifts and intensity changes in the Raman bands characteristic of MAX structures. As an example, the band at 303 cm^{-1} observed for the Mo_2Ga_2C material and attributed to vibrations involving Ga atoms, is shifted to higher Raman shift values (332 cm^{-1}) and its intensity is drastically reduced in the Mo_2CT_x spectrum. This can be explained by the changes in the volume of the lattice with the insertion of the terminal groups in substitution of the Ga atoms. The two main bands observed in the Raman spectrum of Mo_2CT_x (at 143 cm^{-1} and 249 cm^{-1}), assigned to vibrations dominated by Mo atoms, are also shifted as compared to those observed in the corresponding MAX phase (172 cm^{-1} and 229 cm^{-1}) but their intensity is highly increased. Besides, new bands from modes related to both the end groups and the two-dimensional structure of MXenes should also be observed. Indeed, the other less intense bands observed in the Raman spectrum of Mo_2CT_x are mostly related to the presence of oxygen terminal groups [32].

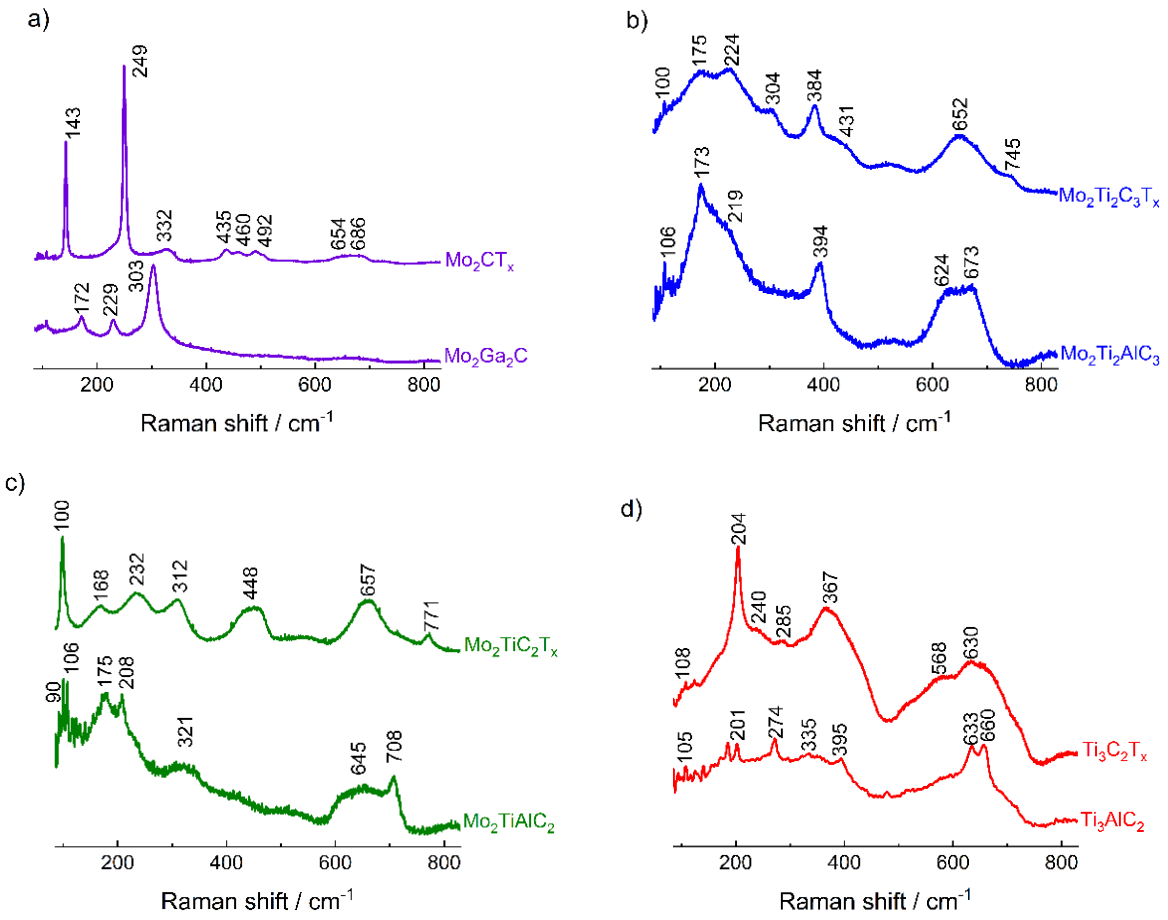

***Figure 9**. Raman spectra of the different MAX and MXene phases.*

The same general features are also observed when comparing the spectra of MXene and corresponding MAX phase for the three other studied cases (**Figure 9 and table S1**):

- For $Mo_2Ti_2C_3T_x$, no bands related to the A-element are observed, the broad bands at low frequency being attributed to modes mainly associated to metal atoms displacements. The band observed at 384 cm^{-1} corresponds to the A_{1g} mode dominated by the displacement of metal atoms (Mo, Ti) observed at 394 cm^{-1} in the corresponding MAX phase. The shoulder at 431 cm^{-1} is probably due to O terminal groups while the two bands observed at 652 and 745 cm^{-1} are due to the displacement of C atoms (parallel and perpendicular to the basal plan). Finally, it should be stated that the obtained spectrum is consistent with the presence of O terminal groups [32].
- For $Mo_2TiC_2T_x$, the sharp peak at 100 cm^{-1} can be assigned to the E_{1g} mode dominated by the displacement of Mo atoms observed at 106 cm^{-1} in the corresponding MAX phase while the A_{1g} mode associated to the displacement of Mo atoms along the c-axis, and observed at 208 cm^{-1} in the spectrum of the MAX phase, is no longer observed. Indeed, the two bands at 168 and 232 cm^{-1} have been ascribed to the presence of O terminal groups. The bands at 312 cm^{-1} and 448 cm^{-1} are also related to the presence of oxygen and the two higher frequency modes are dominated by the displacement of carbon atoms parallel and perpendicular to the basal plane [32].
- For $Ti_3C_2T_x$, the main band at 204 cm^{-1} corresponds to the A1g mode observed at 274 cm^{-1} in the corresponding MAX phase and mainly involving Ti atoms. The important shift is explained by the removal of Al atoms and its replacement by surface terminal groups. The observed position of this band indicates the presence of O terminal groups. The bands observed in the region 230-500 cm^{-1} are related to the in-plane vibrations (Eg) of surface groups bounded to Ti atoms. They indicate, respectively the presence of F (at 240 cm^{-1}), OH (285 cm^{-1}) and O (367 cm^{-1}) terminal groups [6]. Finally, the broad bands observed above 500 cm^{-1} are assigned mostly to vibrations of the C layer.

These bands are also affected by the presence of terminal groups, the position observed herein being indicative of the coexistence of oxygen, hydroxyl and fluorine for $Ti_3C_2T_x$ [6,32,52].

In conclusion, this Raman spectroscopy study confirms the elimination of A-elements of the MAX phases to obtain the MXenes. Moreover, it highlights the greater affinity of Mo for the oxygenated terminal groups.

Surface characterization of MXenes by XPS

XPS is a powerful technique to analyze the MXene surface chemistry, and the chemical environment around a specific element [6,57–59]. The results can then be compared with those obtained by techniques probing the whole sample such as XRD, EDX and ICP-OES.

For the fitting of the spectra, a Shirley background model was selected as it has been shown to be the most suited for the decomposition of spectra recorded with $Ti_3C_2T_x$ [57]. Lorentzian asymmetric functions (LA(x)) were selected for the contributions related to the MXenes whereas Gaussian/Lorentzian symmetric functions were selected for oxides and impurities (see **Tables S3 to S6**). Indeed, asymmetric functions are required for curve fittings of electronic conducting materials such as MXenes [57].

The Mo 3d and Ti 2p regions of the different MXenes were studied (**Figure 10**). As expected, several doublets ($3d_{5/2}$ and $3d_{3/2}$ for Mo and $2p_{3/2}$ and $2p_{1/2}$ for Ti) are observed which is due to spin-orbit coupling and, for simplicity, the following discussion will be based only on the lowest energy photopeak ($3d_{3/2}$ or $2p_{1/2}$).

For all Mo-based MXenes, it is observed that the spectral envelope of Mo 3d photopeak is roughly identical, indicating an equivalent chemical environment for Mo. Two different peaks are used for the spectral decomposition. The first one centered between 229.1 and 229.4 eV and labelled C-Mo-T_x, is attributed to Mo atoms of MXene bounded both to C atoms and to T terminal groups. The second one, centered between 231.5 and 232.2 eV, is ascribed to molybdenum oxide (labelled MoO_x) [33], that is formed during the synthesis. Contrary to the work of Halim *et al.* [33], only one oxide peak was required to fit the Mo 3d region. The partial oxidation of the MXene surface is frequently encountered due to their sensitivity to water and/or air [6], even if these XPS measurements were performed less than 24 h after synthesis. Only specific synthesis under controlled conditions (MXenes prepared by soft etching of MAX film) and storage enables avoiding this partial oxidation [57].

Based on a combination of XANES and XPS, Deeva et al [17] proposed that photopeaks observed at 229.2 eV and 232.2 eV can be assigned to +4 and +5 Mo oxidation states, respectively. However, it is unclear if the contribution at higher BE can be assigned to Mo atoms belonging to the MXene or to an oxide phase. Considering the sensitivity of MXene toward oxidation, we propose to assign this signal to a surface oxide. These discrepancies on the peak assignments could probably be addressed using theoretical calculations to determine if such a +5 oxidation state for Mo can exist in Mo-based MXenes.

The Ti $2p_{1/2}$ region is much more complex since multiple chemical environments for Ti are observed. Focusing on $Ti_3C_2T_x$, four contributions are deduced from the curves fitting:

- at 455.0 eV corresponding to the core Ti atoms surrounded only by C atoms, labelled C-Ti-C,
- at 455.8 eV and 456.8 eV corresponding to surface Ti atoms surrounded by C atoms and terminal groups (O, OH, F), labelled C-Ti^1-T_x and C-Ti^2-T_x,
- at 459.7 eV corresponding to $TiO_{2-x}F_{2x}$ formed by partial oxidation of the surface of the MXene and labelled $TiO_{2-x}F_{2x}$.

The assignment of the 3 asymmetric peaks centered at 455.0 eV, 455.8 and 456.8 eV to a specific bond type is still much debated in the literature and many discrepancies are reported [6,57–62]. Nevertheless, for the quantification of Ti atoms in MXene, the areas of these 3 peaks can be considered, because they can be attributed without any doubt to the Ti atoms belonging to the MXene structure.

Concerning now the $Mo_2TiC_2T_x$ and $Mo_2Ti_2C_3T_x$ MXenes, the contribution at 458.5-458.6 eV is attributed to TiO_2, at a lower binding energy than the $TiO_{2-x}F_{2x}$ contribution observed on $Ti_3C_2T_x$ (459.7

eV). Indeed, the contribution associated to TiO_2 is, in general, observed at around 458.6-458.8 eV [63], whereas the substitution of O for F in the structure, resulting in the formation of $TiO_{2-x}F_{2x}$, leads to a shift of the peak towards higher binding energy (BE) values [63]. Few fluorine atoms are present in $Mo_2TiC_2T_x$ and $Mo_2Ti_2C_3T_x$ in comparison with $Ti_3C_2T_x$, as showed by EDX analyses (**Table 4**) and XPS **(Table S1)**, explaining why TiO_2 is preferentially observed in Mo-containing samples.

Furthermore, it is worth noting that the global envelope including the three peaks used to decompose the Ti 2p region (C-Ti-C, C-Ti^{2+}-T_x, C-Ti^{3+}-T_x) corresponding to the MXene is thinner in the $Mo_2TiC_2T_x$ and $Mo_2Ti_2C_3T_x$ solid solutions compared to $Ti_3C_2T_x$. Indeed, for both, the major contribution corresponds to C-Ti-C, indicating that the majority of titanium atoms are not at the surface, in accordance with the corresponding "ideal" structure (**Figure 11**). However, small fractions of C-Ti^{2}-T_x and TiO_2 are observed indicating the presence of a small amount of Ti atoms at the surface. By adding the C-Ti^{2}-T_x and TiO_2 contributions of XPS curve fittings (**Tables S5 and S6**), it is found that 25% and 24% of the total amount of titanium are at the surface for $Mo_2TiC_2T_x$ and $Mo_2Ti_2C_3T_x$, respectively. This is in good agreement with the quantification obtained by Rietveld refinement of the corresponding Mo_2TiAlC_2 and $Mo_2Ti_2AlC_3$ MAX phases, which led to 24% and 20% of the total amount of Ti atoms substituting Mo atoms in the Mo layer, respectively (**Figure S3-S4**). The correlation between the two methods is rather good showing firstly that MXenes keep their initial MAX structure during their synthesis, as already observed by TEM [13], and secondly that Mo-based MXenes are mainly composed of Mo at the surface. Interestingly, this work also shows that the contribution at 455 eV, with contradictory assignment in the literature [6,57,58,60–62], can be attributed only to the core Ti atoms (titanium surrounded only by carbon atoms) and not to Ti atoms chemically bounded to T groups. Note also that the C-Ti-C contribution slightly shifts to higher BE when the molybdenum content increases from $Ti_3C_2T_x$ (455 eV) to $Mo_2TiC_2T_x$ (455.5 eV) (**Table S4 to S6**). This is probably related to the presence of Mo atoms as second neighbors (after the C atom), the number of Ti-C-Mo units increasing with the Mo content in the MXene (**Figure 11**).

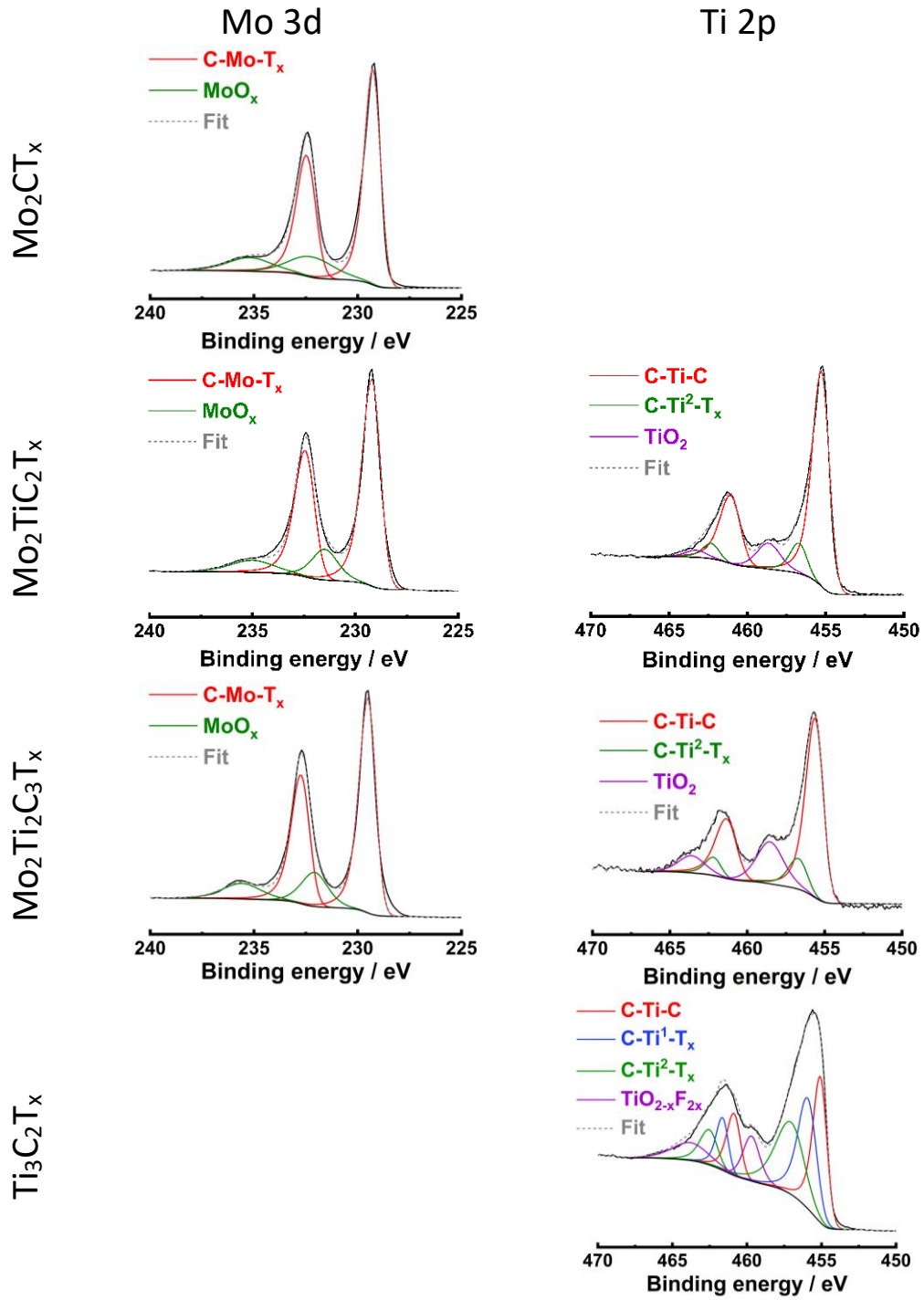

***Figure 10**. High resolution XPS spectra with curve fitting of Mo 3d and Ti 2p regions recorded with the different MXenes whose labels are listed on the left-hand side. For a better visibility, all spectra were normalized to the most intense peak for each region.*

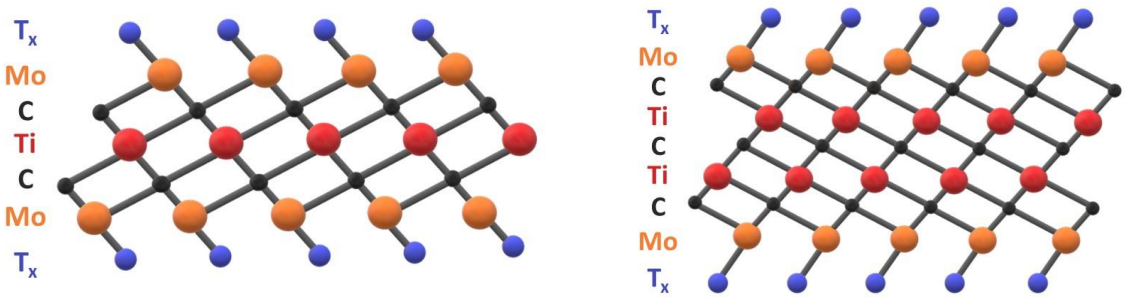

Figure 11. *Schematic representation of the "ideal" structure of $Mo_2TiC_2T_x$ (left) and $Mo_2Ti_2C_3T_x$ (right).*

Focusing now on the C 1s region, three contributions can be observed for $Ti_3C_2T_x$ (**Figure 12**). The first one, centered at 281.9 eV, can be assigned to C atoms bounded to Ti atoms in the MXene and the two others to impurities coming from the synthesis or the surface contamination (adventitious carbon) by exposition to ambient atmosphere (C-C and CH_x) [6,58]. The MXene oxidation can also engender the formation of graphitic/turbostratic carbon which can contribute to the C-C peak used for the decomposition [33]. However, the rate of oxidation is relatively low for all MXenes (see comments of Ti 2p and Mo 3d regions), which cannot explain the high magnitude of this peak. Thus, in addition to surface contamination, it is mostly probable that C-C and CH_x bonds of intercalated TBA^+ cations are responsible for increasing the intensity of these peaks, explaining their relatively high intensity compared to "model" MXenes [57]. These last contributions, encountered very regularly in XPS in the C 1s region, are found on all MXenes (two other low intensity peaks ascribed to C-O and COO groups, have been added for some MXenes, probably linked to other surface contaminations) (**Figure 12**).
Mo-C-Mo and Mo-C-Ti contributions related to the carbon in the MXenes are also observed in the Mo-based MXenes. It is interesting to note that the contribution related to the carbon in the MXene shifts to higher BE when the Mo content increases from $Ti_3C_2T_x$ to Mo_2CT_x. Moreover, this photopeak is broader and can be decomposed into two contributions in the case of $Mo_2Ti_2C_3T_x$. Thus, the following evolution for the BE corresponding to metal-carbon bonds is observed: 281.8 eV ($Ti_3C_2T_x$), 282.0 eV and 282.6 eV ($Mo_2Ti_2C_3T_x$), 282.9 eV ($Mo_2TiC_2T_x$) and 283.1 eV (Mo_2CT_x). To explain the different contributions and shifts, it is necessary to look at the structures. In $Ti_3C_2T_x$, there is only one type of C atoms surrounded by Ti atoms and only one peak labelled Ti-C-Ti is used for the decomposition of the XPS spectrum (**Figure 12**). In Mo_2CT_x, C atoms are only surrounded by Mo atoms leading to a shift at higher BE of the peak labelled Mo-C-Mo in comparison with Ti-C-Ti peak. In the case of $Mo_2TiC_2T_x$, C atoms are surrounded both by Ti and Mo atoms (**Figure 11**), and the BE associated to the corresponding peak, labelled Mo-C-Ti, is logically in between the BE of Ti-C-Ti and Mo-C-Mo peaks (**Table S5**). Two different chemical environments for C atoms are observed in $Mo_2Ti_2C_3T_x$ (**Figure 11**): one for which C atoms are surrounded with Ti atoms (corresponding to Ti-C-Ti peak) and a second one for which C atoms are surrounded both by Ti and Mo atoms (corresponding to Mo-C-Ti peak). This is in agreement with the study reported by Halim *et al*. [33]. Interestingly, the area ratio for the two peaks (**Table S6**) is equal to 2.1, that is to know close to the theoretical ratio of 2 obtained with the ideal structure (2 Mo-C-Ti for 1 Ti-C-Ti) confirming peak assignments. The C 1s region is thus an extremely interesting probe to study and confirm the structural evolution of MXenes as a function of molybdenum content.

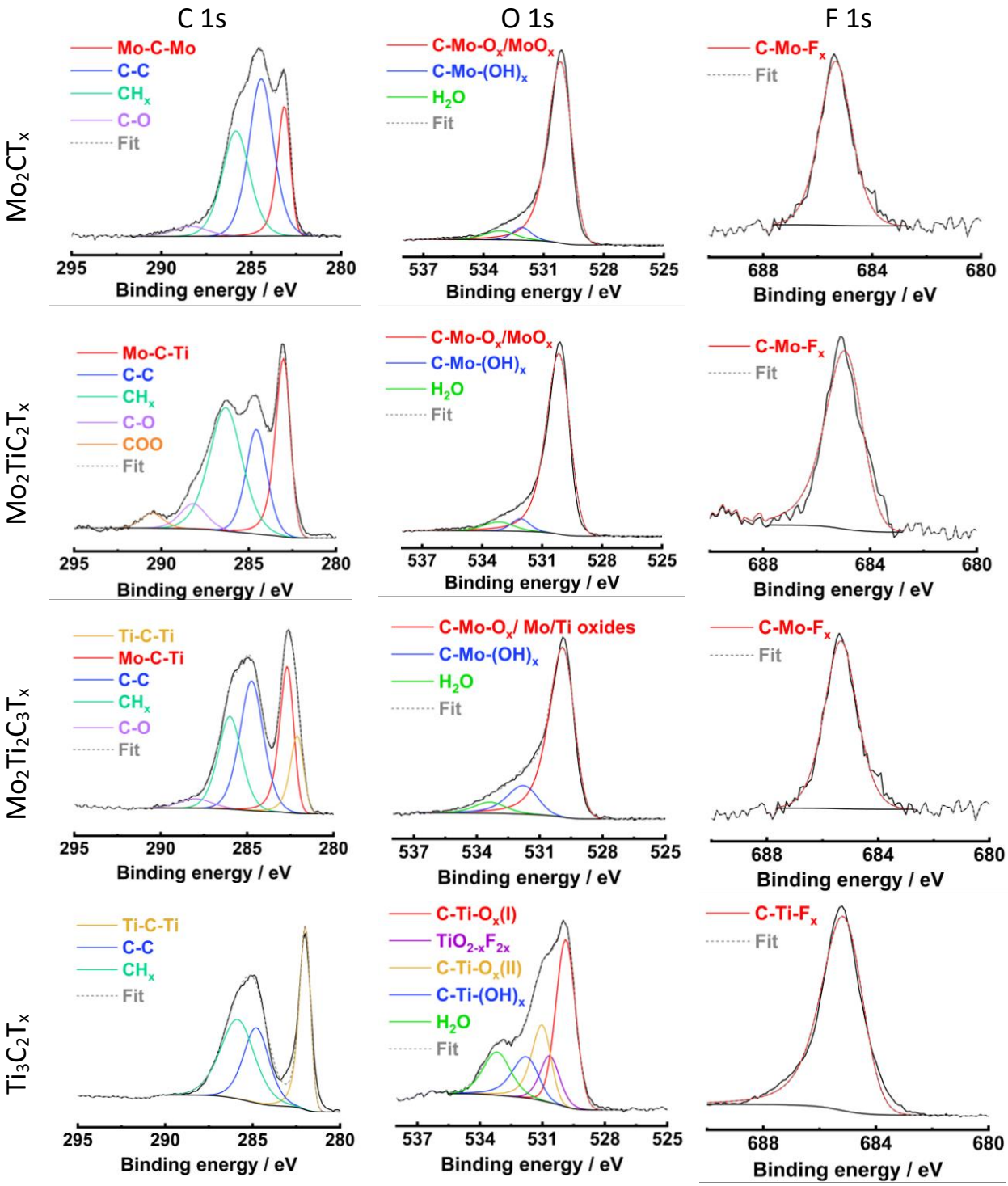

***Figure 12**. High resolution XPS spectra with curve fitting of C 1s, O 1s and F 1s regions recorded with the different MXenes whose labels are listed on the left-hand side. For a better visibility, all spectra were normalized to the most intense peak for each region.*

The O 1s region is much more complex. Indeed, several assignments have been proposed in the literature due to the nature of terminal groups (-O, -OH), the nature of the crystallographic sites occupied by oxygen terminal group in the MXene structures (bridge or fcc), the presence of oxides (TiO_2, $TiO_{2-x}F_{2x}$ and/or MoO_x), impurities (OR) and water [6,33,57,58,61]. Several peaks ascribed to the previously mentioned contributions can also overlap. This complicates the decomposition of O 1s

region since more contributions than those observed by *Näslund et al.* on a "model" MXene are required [57].

Looking at the O 1s region of $Ti_3C_2T_x$, the contribution at 529.8 eV, named C-Ti-$O_{x(I)}$ is attributed to oxygen terminal group of MXene in a bridge site [6,57,61]. We can exclude the presence of oxygen of TiO_2 in this contribution since the presence of this oxide was not evidenced in the Ti 2p region. The contribution at 530.6 eV is attributed to the oxygen belonging to $TiO_{2-x}F_{2x}$ phase, identified in the Ti 2p region, as evidenced clearly by previous works done by some of us on oxidized MXenes [6]. Based on the work of Näslund *et al.* [57], the photopeak at 530.9 eV, labelled C-Ti-$O_{x(ii)}$ should be attributed to oxygen terminal group in the fcc sites. The photopeak at 531.9 eV, labelled C-Ti-$(OH)_x$ is attributed to -OH terminal groups. This kind of terminal group is not systematically observed on MXene by XPS [57]. However, the formation of –OH terminal groups seems to be favored when using a concentrated HF etching agent (as in the present work) as previously evidenced by combining XPS and Raman analyses on $Ti_3C_2T_x$ MXenes prepared with different etching agents [6]. The last peak centered at 533.2 eV is attributed to adsorbed and/or intercalated water molecules. Nevertheless, the presence of oxygenated organic impurities, often encountered at 533-534 eV, cannot be excluded.

For Mo-based MXene, the shape of the O 1s envelope is similar for the three samples indicating once again a roughly identical surface chemistry. The photopeak at 529.8-530 eV is attributed to -O terminal group bounded to Mo [33], but, unfortunately, this peak may also be associated to O atoms from MoO_x and TiO_2 oxides. In their works, Halim *et al.* identified a contribution at 531 eV related to O atoms in the fcc site [33]. This contribution is not observed herein probably indicating that all terminal groups are in the same crystallographic site for Mo-based MXenes. As in the work of Halim *et al.* [33], the contribution of -OH terminal groups is observed at ca. 532.0 eV. Finally, O-atoms from water molecules are responsible for the signal observed at 533-534 eV.

However, the assignment of the different photopeaks in the O 1s region remains debatable and argues for theoretical calculations, especially concerning the influence of the nature of the crystallographic sites occupied by the terminal groups on the BE.

For the F 1s region (**Figure 12**), the only observed peak is attributed to -F terminal group bounded to Mo for Mo_2CT_x, $Mo_2TiC_2T_x$ et $Mo_2Ti_2C_3T_x$ and to Ti for $Ti_3C_2T_x$ as observed by Halim *et al*. [33]. It is labelled C-M-F_x with M = Mo or Ti. However, this photopeak includes the contribution of F atoms from $TiO_{2-x}F_{2x}$ in the case of $Ti_3C_2T_x$. As expected, for Mo-based MXene, the magnitude of the signal in the F 1s region is very low as illustrated by the more important background in comparison with the spectrum recorded with $Ti_3C_2T_x$. This is confirmed by the overall contents of each element determined by XPS (**Table S2**).

By only considering photopeaks ascribed to atoms composing MXenes, a quantification has been proposed and is reported in **Table 6**. Calculations have been performed on the basis of data obtained from the decomposition of the different high resolution XPS spectra. These data are given in **Tables S2 to S6**. The element contents have been normalized to two Mo atoms for Mo-containing MXenes or to three Ti atoms for $Ti_3C_2T_x$. By only focusing on the Mo, Ti and C elements, the obtained compositions (*i.e.* Mo_2C, $Mo_2Ti_{0.8}C_{2.5}$, $Mo_2Ti_{1.8}C_{3.2}$ and $Ti_3C_{2.2}$) are close to the expected ones (*i.e.* Mo_2C, Mo_2TiC_2, $Mo_2Ti_2C_3$ and Ti_3C_2) considering the significant uncertainty of the method. Thus, the surface (XPS) Mo/Ti/C ratios don't differ from the bulk ratios (ICP-OES/EDX).

Still, in their work, Halim *et al*. [33] observed a significant decrease in Ti and C contents for Mo/Ti MXenes finding $Mo_2Ti_{0.6}C_{1.2}$ and $Mo_2Ti_{1.1}C_{1.6}$ stoichiometries. They attributed it to the oxidation of the Ti atoms substituting Mo atoms in the surface layer during the synthesis and/or during the delamination step. Indeed, the TiO_2 fractions observed by XPS on $Mo_2TiC_2T_x$ and $Mo_2Ti_2C_3T_x$ (45% and 32% respectively) are drastically larger than those obtained in this work (22% and 12%, **Tables S5 and S6**). However, this explanation is not entirely satisfactory since it would mean that almost half of Ti atoms is in the Mo surface layer , which is not the case [33], showing that a part of core Ti atoms is also oxidized. To explain the higher degree of MXene oxidation in ref [33] in comparison with our samples, a focus should be set on the applied synthesis protocols. While the synthesis parameters are very close (concentrated HF, similar temperature and duration, TBAOH step), the major difference between the two synthesis protocols is the final drying step. It is performed at ambient temperature

and under air in the present work whereas it has been carried out at 200 °C under vacuum in ref [33]. This temperature is quite high and could favor the partial oxidation of the surface Ti atoms subsequently to a reaction with adsorbed/inserted water and/or with -O terminal groups, leading to the formation of TiO_2 and amorphous carbon. This would therefore decrease the Ti and C contents included in the MXene. MXene can be oxidized over time even under inert atmosphere by reaction with intercalated water [6]. Such an oxidation process is kinetically favored at 200°C. Thus, the drying step impacts MXene properties. This is especially true for Mo/Ti MXenes since the reactivity of Ti and Mo toward oxidation is different.

Concerning now the terminal groups (**Table 6**), the quantification is quite difficult due to the overlapping of the different species, especially in the O 1s region. For quantification, the oxygen content of the molybdenum oxide in the peak centered at 529.8 eV where C-Mo-O_x appears, was subtracted. To do this, MoO_3 is considered as the oxide and the oxygen amount is determined from the peak area in the Mo 3d region attributed to this oxide considering 3 O for 1 Mo. Likewise, for $Ti_3C_2T_x$, the amount of F atoms belonging to $TiO_{2-x}F_{2x}$ should be subtracted from the area of C-Ti-F_x peak centered at 685.0 eV. To do this, the x value of $TiO_{2-x}F_{2x}$ has been determined by combining the area of peaks ascribed to $TiO_{2-x}F_{2x}$ in the Ti 2p and in the O 1s regions (459.7 and 530.6 eV respectively) and by considering an oxidation state of 4 for titanium. Thus, a composition of $TiO_{0.46}F_{3.08}$ was obtained allowing to subtract the amount of F atoms belonging to the oxyfluoride phase from the signal ascribed to C-Ti-F_x.

In **Table 6**, z corresponds to the sum of terminal groups per $M_{n+1}X_n$ unity. It is well established that this value should be close to 2 [60,64]. Using our quantification approach, the obtained z value is close to 2 except for Mo_2CT_x where z = 1.2. No explanation can be brought for the low z value of Mo_2CT_x at this stage. It is not required to consider the substitution of C by O atoms in the MXene structure to get a z value closer to the expected one, contrary to what was proposed in the work of Halim *et al.* [33]. Substitution of C for O atoms was proposed in reason of the high oxidation degree of MXenes, mechanically leading to the reduction of the C content and offering space for O insertion. In the present work, no evidence for the formation of C vacancies can be provided.

Even if the obtained quantification for terminal groups by XPS is satisfactory considering the reasonable z values in comparison with the expected ones, the uncertainty of the method and the various assumptions made for this quantification encourages to take it with caution. Thus, XPS quantification for T groups should be considered as a semi-quantification method allowing comparing the nature and amounts of T groups between different MXenes rather than an accurate method enabling determining the absolute amounts of each T group. Moreover, this quantification is only related to the surface and not to the bulk. However, major results can be obtained: (i) the formation of -F terminal groups is favored by the presence of Ti at the surface (case of $Ti_3C_2T_x$) showing the higher affinity of this element for fluorine (ii) the fraction of each terminal groups is relatively close for the three Mo-based MXenes with a majority of oxygenated terminal groups. Thus, similar surface properties are expected for these three samples.

Table 6: *Determination of the stoichiometry of the different investigated MXenes on the basis of data recovered from the fitting of high resolution XPS spectra (**Tables S3 to S6**) and from the global content of elements (**Table S2**). The results are normalized for 2 Mo atoms (Mo-containing MXenes) or 3 Ti atoms ($Ti_3C_2T_x$). z is the sum of terminal groups.*

MXene	Mo	Ti	C	O	OH	F	z
Mo_2CT_x	2	-	1.0	0.9	0.1	0.2	1.2
$Mo_2TiC_2T_x$	2	0.8	2.5	1.3	0.2	0.4	1.9
$Mo_2Ti_2C_3T_x$	2	1.8	3.2	1.1	0.5	0.5	2.1
$Ti_3C_2T_x$	-	3	2.2	1.2	0.3	0.9	2.4

To conclude, the major information obtained from XPS analyses are summarized below:

- The sequencing of the Mo, Ti and C layers in the different studied MXenes is confirmed and remain equivalent to those of the corresponding MAX phases.
- As reported for the "ideal" structure, Mo layers are mainly occupied by Mo atoms in the Mo/Ti MXenes. The low fraction of Ti atoms substituting Mo atoms in the Mo layer observed in the initial MAX phases are also observed in the corresponding MXenes. The Mo/Ti ratio in this layer is preserved after exfoliation and delamination.
- The M/X ratios of the $M_{n+1}X_n$ block obtained from XPS data (scan of ≈ 3 layers) agrees with chemical analyses performed using ICP-OES, indicating that core and surface composition are close to each other.
- The surface (terminal groups) of all Mo-containing MXenes are similar in terms of chemical composition.
- According to results obtained from Raman spectroscopy, Ti has a greater affinity for -F terminal group than Mo when it is at the surface.

This in-depth study provides a better understanding of the XPS data reported in literature for Mo/Ti-based MXenes and could potentially be used as a guide to analyze data from other MXenes containing several M elements.

3.3 Electrochemical behavior of MAX/MXenes

The electrocatalytic properties of the different MAX and MXene materials were investigated in alkaline medium (KOH 1 M) in order to correlate them with their surface chemistries. Cyclic voltammograms recorded with MAX and MXenes are shown in **Figure 13**. For all the MAX phases (**Figure 13a**), an irreversible oxidation peak centered at about 1 V *vs.* RHE is observed, corresponding to the oxidation of Ti and/or Mo atoms exposed to the electrolyte, since there is no other redox active species. In the voltammograms of Ti_3AlC_2 and Mo_2Ga_2C, the oxidation peaks are observed at 1.06 and 0.95 V *vs.* RHE respectively indicating that potentials required for the oxidation of Mo and Ti atoms are quite close.
The coulometry associated to this irreversible oxidation is very different from one sample to another. It is higher for the solid solution MAX phases and lower for Mo_2Ga_2C and Ti_3AlC_2 **(Figure 13a**). The charge associated to this redox peak depends on both the number of electrochemically accessible surface atoms and to the number of electrons exchanged for the oxidation of a single atom. If we assume that the number of electrons exchanged per surface metal atoms is the same for Ti and Mo atoms (formation of TiO_2 and MoO_2 respectively), the higher is this charge, the higher is their amount. Based on the previous assumptions, the observed differences can have two different origins:
(i) the electrochemical active surface is different which could result from changes of the powder macroscopic properties (grain sizes, agglomeration,…) requiring complementary analyses (statistic study by microscopy of grains sizes, laser granulometry, N_2 sorption…) to confirm this hypothesis; (ii) the surface of the studied MAX phases is partially oxidized before recording cyclic voltammograms, which reduces the amount of non-oxidized metal atoms.
Whatever the reason, assuming that the number of exchanged electrons per exposed metal atom is the same for all Mo-based MAX (Mo is mainly at the surface for the 3 MAX phases), the amount of accessible non-oxidized Mo sites is drastically higher in Mo_2TiAlC_2 and $Mo_2Ti_2AlC_3$ compared to Mo_2Ga_2C.
Surprisingly, a second peak is observed at lower potential for $Mo_2Ti_2AlC_3$, probably linked to the presence of metal atoms with different sensitivity toward oxidation. At this stage, no explanation can be proposed for this peak.

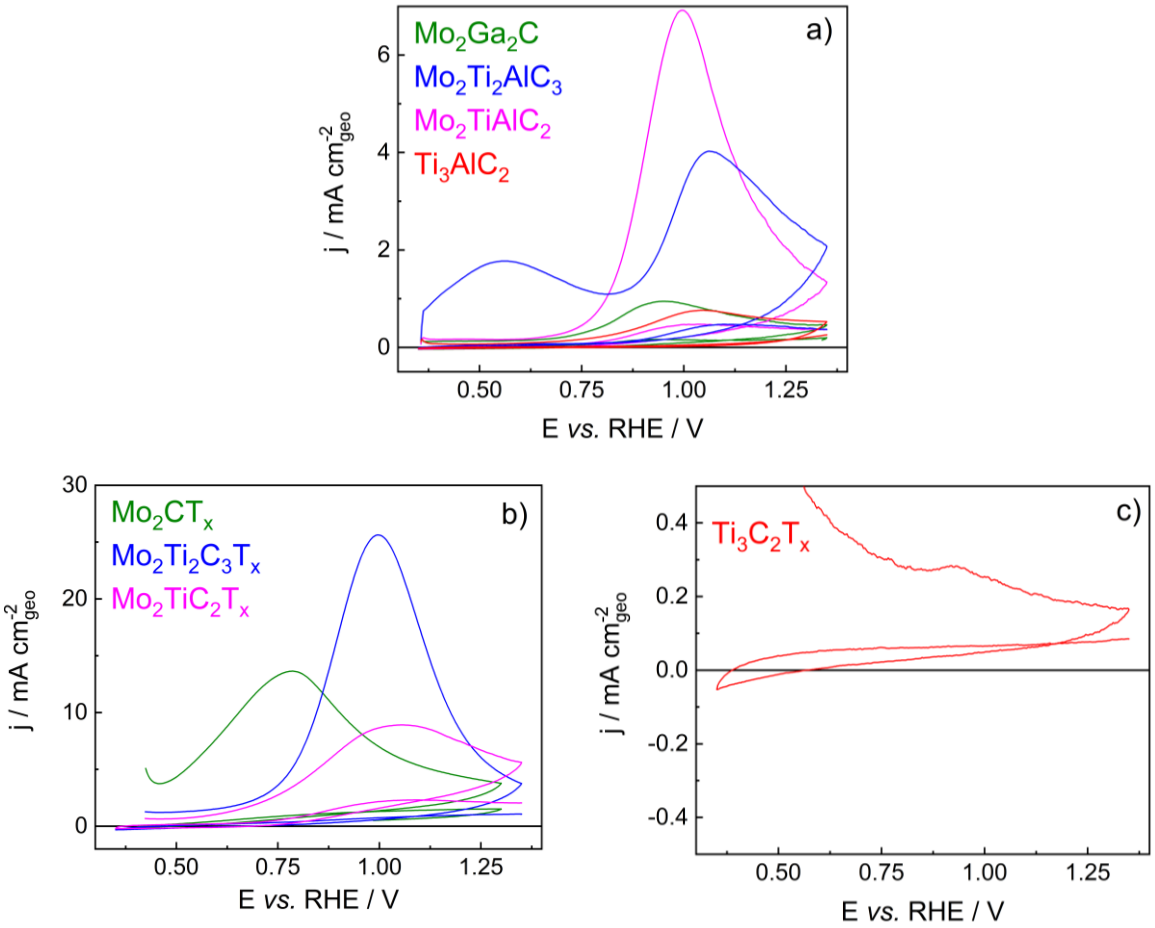

***Figure 13**. Cyclic voltammograms recorded with a) MAX phases, b) Mo_2CT_x $Mo_2TiC_2T_x$, $Mo_2Ti_2C_3T_x$ and c) $Ti_3C_2T_x$ (only the first cycle is reported for clarity). All curves are recorded in a N_2 saturated 1 mol L^{-1} KOH electrolyte. Scan rate 50 mV s^{-1}.*

This irreversible oxidation peak is also observed for the Mo-based MXenes at the same potential as the MAX phases (around 1 V *vs.* RHE) except for Mo_2CT_x (≈ 0.8 V *vs.* RHE) **(Figure 13b)**. More importantly, the coulometry of the Mo-based MXenes is drastically higher than their corresponding MAX phase, indicating a higher amount of accessible metal atoms. This is clearly due to the 2D nano-structuration of the MXenes compared to the 3D structure of the MAX phases, increasing the number of metal atoms in contact with the electrolyte.

On the contrary, the charge associated to the surface oxidation of $Ti_3C_2T_x$ is very low. This low coulometry can be explained by two reasons: (i) a high degree of surface oxidation of the MXene before recording cyclic voltammograms or (ii) a low number of Ti atoms in contact with the electrolyte. Regarding XPS data and more precisely the Ti 2p region (**Figure 10**), the fraction of oxidized Ti atoms (14 % - **Table S4**) is not high enough to explain this low coulometry. The oxidation of MXene during the preparation of the catalytic ink cannot be totally excluded but this phenomenon was never observed with other inks containing $Ti_3C_2T_x$ MXenes in our previous works [6]. The cyclic voltammogram recorded with $Ti_3C_2T_x$ was compared with those obtained with $Ti_3C_2T_x$ prepared with HF 48 w% but without performing the delamination step using TBAOH treatment (sample labelled $Ti_3C_2T_x$ – HF48) and with LiF/HCl etching agent (sample labelled $Ti_3C_2T_x$ – LiF/HCl) (**Figure S10)**. These two last MXenes were prepared according to our previous work [6]. For these two samples, the rate of oxidized Ti atoms determined by XPS is respectively of 10% and 13% [6], that is to know close to the oxidation rate of $Ti_3C_2T_x$ MXene. Though the oxidation rate is the same, the charge associated with the oxidation peak is drastically lower for $Ti_3C_2T_x$. As explained previously, this MXene is not delaminated though TBA^+ ions are inserted between the sheets, in reason of a high interaction between TBA^+ and the surface of

$Ti_3C_2T_x$. Therefore, the inserted TBA^+ in high interaction with the surface prevents the insertion of the electrolyte between the sheets leading to a low number of Ti atoms in contact with the electrolyte.

The catalytic performances of MAX/MXenes were determined towards hydrogen evolution reaction in alkaline medium (**Figure 14)**. These performances were compared with those of a reference material, *i.e.* platinum (40 wt.%) supported on carbon, labelled Pt-C (40%). Onset potentials as well as Tafel slope values are reported in **Table 7**. Onset potentials are approximated by the electrode potential value required to drive a current density of 3 mA cm^{-2}_{geo}.

Table 7: *HER kinetic parameters obtained with different MAX and MXenes. The results are compared with those of a reference catalyst Pt/C (40wt%).*

	samples	E@-3 mA.cm^{-2} (V/RHE))	Tafel slope (mV dec^{-1})
MAX	**Mo_2Ga_2C**	-0.42	94
	Mo_2TiAlC_2	-0.36	77
	$Mo_2Ti_2AlC_3$	-0.37	76
	Ti_3AlC_2	<-0.6	137
MXene	**Mo_2CT_x**	-0.22	84
	$Mo_2TiC_2T_x$	-0.31	83
	$Mo_2Ti_2C_3T_x$	-0.27	85
	$Ti_3C_2T_x$	<-0.6	201
	$Ti_3C_2T_x$-LiF/HCl *	-0.45	180
	$Ti_3C_2T_x$-HF48 *	-0.50	195
	Pt-C (40%)	-0.03	28

** from ref* [6]

MAX phases containing both Mo and Ti elements are more active towards HER than monometallic MAX phases. The onset potentials are indeed of -0.36 and -0.37 V *vs.* RHE for Mo_2TiAlC_2 and $Mo_2Ti_2AlC_3$ respectively (**Figure 14** and **Table 7**). The Ti_3AlC_2 MAX phase exhibits a poor activity, the onset being lower than -0.7 V vs. RHE. Mo-containing MAX phases are largely more efficient, thus confirming that Mo is a better active site for HER than Ti. Indeed, molybdenum carbide is studied for HER contrary to titanium carbide [22,35].

The Tafel slopes values, characteristic of the number of electrons exchanged before the rate determining step, were determined and reported **Figure 14** and **Table 7**. As expected, the MAX phases containing molybdenum have lower Tafel slopes, between 75 and 90 mV dec^{-1} whereas the value is higher for Ti_3AlC_2 (137 mV dec^{-1}). For all these materials the rate determining step is probably the Volmer step (adsorption and dissociation of water molecules). In addition, the involved active sites and reaction mechanisms are similar between the Mo-based MAX phases since an equivalent Tafel slope is obtained. Thus, the difference in HER activity between the three Mo-based MAX is mainly due to the amount of metal sites exposed to the electrolyte. Indeed, as discussed previously, the low coulometry of Mo_2Ga_2C compared to the Mo/Ti MAX phases (**Figure 13**) indicates a lower amount of accessible metallic sites and thus, a lower activity.

Whatever the MAX/MXene system, the HER activity is clearly improved by the formation of the MXenes with an increase of the potential required to drive a current density of -3 mA cm^{-2}_{geo} by ca. 100 mV (**Figure 14b – Table 7**). This is certainly due to the 2D nanostructuration allowing increasing the number of electrochemically accessible metal active sites, in accordance with the respective amount of charges required to oxidize the electrochemically accessible surface metal atoms (**Figure 13**). For example, the potential required to drive a current density of -3 mA cm^{-2}_{geo} is only of -0.22 V *vs.* RHE for Mo_2CT_x and of -0.42 V *vs.* RHE for Mo_2Ga_2C.

The activity of $Ti_3C_2T_x$ MXene is very low (onset potential < - 0.6 V *vs.* RHE) as expected, since this material combines a limited number of metal atoms exposed to the electrolyte with a poorly active Ti-based site. By comparing with $Ti_3C_2T_x$ – HF48 and $Ti_3C_2T_x$ – LiF/HCl [6], the obtained performances are

drastically lower confirming the low accessibility of titanium active site in this specific $Ti_3C_2T_x$ MXene (**Figure 14b – Table 7**). Anyway, the Mo-based MXenes exhibit a better HER activity and a lower Tafel slope value (**Figure 14d – Table 7**) than the different $Ti_3C_2T_x$ MXenes.
Among the Mo-based MXene, Mo_2CT_x is the more active for HER with the higher onset potential value (**Figure 14b – Table 7**). The three MXenes have similar Tafel slopes values, around 80-85 mV dec^{-1}, close to those obtained for the corresponding MAX phase (75-90 mV dec^{-1}) indicating an equivalent rate determining step and thus a similar active site, *i.e.* Mo atom, for the MAX and MXene phases. This last result is of upmost interest. Indeed, it seems possible to predict the activity of MXenes just by measuring those of the corresponding MAX phases, if we are able to consider accessibility issue (grain size, etc.) when comparing the activity of the different MAX phases.

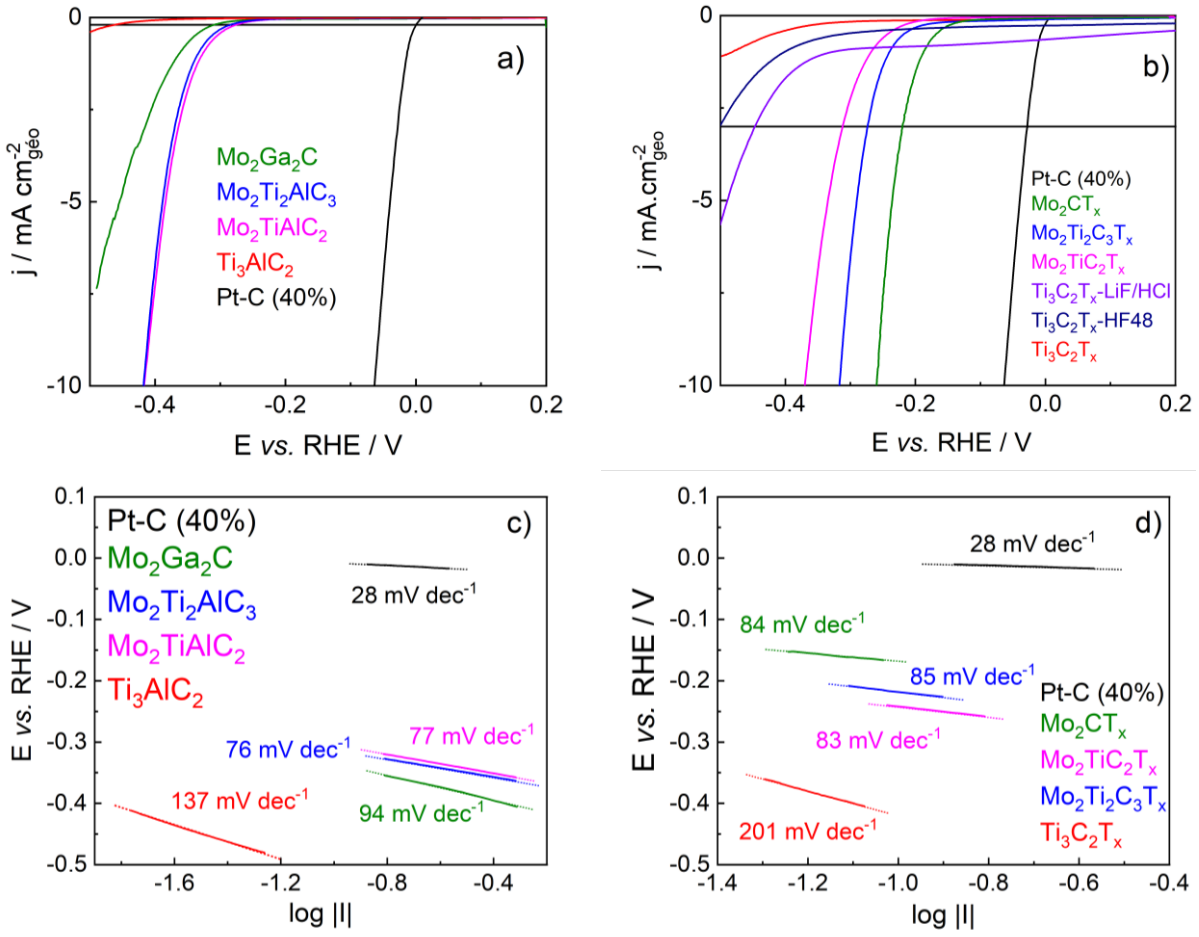

***Figure 14**. HER polarization curves recorded with a) MAX phases and b) MXenes. All curves are recorded in a N_2 saturated 1 mol L^{-1} KOH electrolyte at a scan rate of 5 mV s^{-1} Tafel slopes extracted from the polarization curves for c) MAX and b) MXene catalysts.*

The difference between the three Mo-based MXenes is high enough to be underlined, since the onset potential value is of - 0.22, -0.31 and -0.27 V *vs.* RHE for Mo_2CT_x, $Mo_2TiC_2T_x$ and $Mo_2Ti_2C_3T_x$, respectively. As discussed above, Mo is the best active site and, therefore, Ti atoms have no or little influence on the HER activity in the $(Mo,Ti)_{n+1}C_nT_x$ phases. The activity per Mo site for HER is probably equivalent between each sample since the electronic charge of the Mo is the same as highlighted by XPS (same BE of C-Mo-T_x - **Figure 10)**. Thus, the activity difference is related to the amount of accessible Mo in the sample. This amount cannot be simply estimated with the amount of charge associated with the oxidation of surface metal atoms (**Figure 13**), since it can be ascribed to surface Mo and Ti atoms

oxidation for the Mo/Ti phases. Such an estimation can only be performed with Mo_2CT_x. However, one can proceed by first principle thinking as follows. The amount of charge required to oxidize Mo_2CT_x surface atoms is lower than for $Mo_2Ti_2C_3T_x$ (68.4 and 124.2 mC, respectively). This indicates that the lower HER activity of $Mo_2Ti_2C_3T_x$ can be attributed to the substitution of Mo atoms for Ti atoms at the surface of $Mo_2Ti_2C_3T_x$ (12% of the total amount of Ti, based on the C-Ti^2-T_x contribution in XPS, **Table S6**), reducing the amount of electrochemically active Mo atoms per $M_{n+1}C_nT_x$ formula. In other words, if the metal surface layer was completely occupied by Mo atoms in $Mo_2Ti_2C_3T_x$, a higher HER activity should be obtained. The lower HER activity of $Mo_2TiC_2T_x$ in comparison with Mo_2CT_x and $Mo_2Ti_2C_3T_x$ is probably due to both the presence of Ti (13% of the total amount of Ti, based on the C-Ti^2-T_x contribution in XPS, **Table S4**) and to a significantly lower active surface area (the charge associated to irreversible oxidation peak is 37.6 mC). At this stage, the difference in accessibility for these different MXenes is difficult to determine since it can depend on a combination of factors, such as size of sheets, rate of delamination and/or sheets stackings. This indicates also that the chemical composition should not be the only factor to consider when comparing HER performances of different MXenes.
Finally, the HER activity is clearly lower than for Pt-C (40%) even considering the best MXene catalyst, *i e.* Mo_2CT_x (**Figure 14b – Table 7**). Nevertheless, MXene is free from noble metals, a clear advantage from an industrial point-of-view. However, increasing the HER activity of such materials is still necessary to use it in an electrolysis cell capable of working at current densities in the range of 1 A cm^{-2} with a cell voltage lower than 1.9 - 2.0 V. Two research directions can be therefore considered: increasing the amount of accessible Mo sites by adapting the synthesis process (rate of delamination, size of sheets, bridging of sheets [65] with a spacer to facilitate the electrolyte diffusion…) or using highly electron conducting MXenes as efficient co-catalyst support. Some of us have already proposed it by preparing MoS_2@Mo_2CT_x composites, that is very efficient towards HER in alkaline medium [23]. It will also be important to look at the long-term stability of these Mo-based MXenes under HER conditions in an alkaline medium in order to verify that it remains stable unlike their use under ORR conditions [66].

4. Conclusion

In this work, different Mo/Ti solid solution-based MAX and MXenes were successfully synthesized and characterized. The MAX phases have an excellent purity (≥ 97%) and an expected structural configuration. However, the presence of Ti atoms in the Mo layers was highlighted for Mo_2TiAlC_2 and $Mo_2Ti_2AlC_3$ solid solution MAX phases. The synthesis of the corresponding MXenes was performed in concentrated HF as etching agent followed by immersion in TBAOH, leading to delaminated sheets thanks to the insertion of TBA^+ and H_2O between the sheets. Whereas the etching of Al is total for Al-based MAX phases with adapted conditions, this TBAOH step is also essential to separate the MXene from the non-reacted MAX phase in the case of Mo_2CT_x, since Mo_2Ga_2C phase is more refractory toward etching because of the strong Mo-Ga bond.
The sequencing of layers and the $M_{n+1}X_n$ chemical composition of the initial MAX phases are preserved in the MXenes. The molybdenum atoms are mainly found on the surface of the sheets for the three MXenes Mo_2CT_x, $Mo_2TiC_2T_x$ and $Mo_2Ti_2C_3T_x$ even if a small but not insignificant amount of Ti atoms is also observed at the surface for the $(Mo,Ti)_{n+1}C_nT_x$ phases. The C 1s analysis by XPS is a performant probe for study and confirm the structural evolution of MXenes as a function of the Mo content.
The electronic charge and the chemical environment of Mo determined by XPS is the same for the 3 Mo-based MXenes, leading to equivalent surface properties such as those involved in electrocatalysis. Whereas $Ti_3C_2T_x$ MXene have a high affinity toward -F as terminal groups, the Mo-based MXenes favor the formation of oxygenated groups in the investigated synthesis conditions.
The 2D nano-structuration by forming MXenes allows to improve considerably the activity against hydrogen evolution reaction in alkaline medium compared to their corresponding MAX phase, thanks to an increase of the active sites amount. However, since MAX phases are more common, comparing MAX phases to each other is a viable option to get an idea of which MXene will be the most active.

Mo-based MXenes are more active than $Ti_3C_2T_x$, whatever the method of synthesis for the latter, indicating that molybdenum in carbide form is a much better active center than titanium carbide. Although Mo_2CT_x is the most active catalyst for HER in alkaline medium with an onset at -3 mA cm^{-2}_{geo} of - 0.22 *vs.* RHE, the use of $(Mo,Ti)_{n+1}C_nT_x$ phases, particularly $Mo_2Ti_2C_3T_x$, is a credible alternative of Mo_2CT_x, since their surface properties are similar, even if the presence of Ti atoms reduces the catalytic performances. Indeed, the synthesis of $(Mo,Ti)_{n+1}C_nT_x$ MXenes requires lower duration and leads to higher yields in the reported synthesis conditions, a great advantage from an industrial point of view, possibly compensating for the loss in activity. Thus, these materials can be considered as efficient active support for hydrogen evolution reaction. Finally, the combined in-depth characterizations done in this work aims also as serving as a guide for the MXene community to better understand their experimental signals obtained on different MXenes.

Acknowledgments

The authors acknowledge financial support from the “Agence Nationale de la Recherche” (references ANR-18-CE08-014 – MXENECAT project and ANR-22-CE08-0014 – PIXIES project). The authors acknowledge the European Union (ERDF) and Région Nouvelle Aquitaine for the funding of MABATRI (reference 2021-16148810) and PLATABAT (reference 2022-291111-POC) projects. This work pertains to the French government program "Investissements d'Avenir" (EUR INTREE, reference ANR-18-EURE-0010). The authors wish to thanks S. Arrii for XRD experiments.

Appendix A. Supplementary data

Rietveld refinement of X-Ray diagrams; SEM pictures of MAX phases; XRD patterns of $Mo_2TiC_2T_x$ and $Mo_2Ti_2C_3T_x$ after etching in HF 48% during 24 h; Pictures of MXenes after filtration; Comparison of MXene prepared with and without TBAOH step; Assignment of the Raman bands in MAX phases; XPS analyses of MXenes; Cyclic voltammograms comparison for different $Ti_3C_2T_x$ MXenes.

References

[1] M. Naguib, M. Kurtoglu, V. Presser, J. Lu, J. Niu, M. Heon, L. Hultman, Y. Gogotsi, M.W. Barsoum, Two-Dimensional Nanocrystals Produced by Exfoliation of Ti3AlC2, Advanced Materials. 23 (2011) 4248–4253. https://doi.org/10.1002/adma.201102306.

[2] A. VahidMohammadi, J. Rosen, Y. Gogotsi, The world of two-dimensional carbides and nitrides (MXenes), Science. 372 (2021). https://doi.org/10.1126/science.abf1581.

[3] Y. Gogotsi, B. Anasori, The Rise of MXenes, ACS Nano. 13 (2019) 8491–8494. https://doi.org/10.1021/acsnano.9b06394.

[4] M. Naguib, M.W. Barsoum, Y. Gogotsi, Ten Years of Progress in the Synthesis and Development of MXenes, Advanced Materials. 33 (2021) 2103393. https://doi.org/10.1002/adma.202103393.

[5] M. Downes, C.E. Shuck, R.W. Lord, M. Anayee, M. Shekhirev, R.J. Wang, T. Hryhorchuk, M. Dahlqvist, J. Rosen, Y. Gogotsi, M5X4: A Family of MXenes, ACS Nano. 17 (2023) 17158–17168. https://doi.org/10.1021/acsnano.3c04967.

[6] M. Benchakar, L. Loupias, C. Garnero, T. Bilyk, C. Morais, C. Canaff, N. Guignard, S. Morisset, H. Pazniak, S. Hurand, P. Chartier, J. Pacaud, V. Mauchamp, M.W. Barsoum, A. Habrioux, S. Célérier, One MAX phase, different MXenes: A guideline to understand the crucial role of etching conditions on Ti3C2Tx surface chemistry, Applied Surface Science. 530 (2020) 147209. https://doi.org/10.1016/j.apsusc.2020.147209.

[7] X. Wang, C. Garnero, G. Rochard, D. Magne, S. Morisset, S. Hurand, P. Chartier, J. Rousseau, T. Cabioc'h, C. Coutanceau, V. Mauchamp, S. Célérier, A new etching environment (FeF3/HCl) for the synthesis of two-dimensional titanium carbide MXenes: a route towards selective reactivity vs. water, J. Mater. Chem. A. 5 (2017) 22012–22023. https://doi.org/10.1039/C7TA01082F.
[8] Y. Xie, M. Naguib, V.N. Mochalin, M.W. Barsoum, Y. Gogotsi, X. Yu, K.-W. Nam, X.-Q. Yang, A.I. Kolesnikov, P.R.C. Kent, Role of Surface Structure on Li-Ion Energy Storage Capacity of Two-Dimensional Transition-Metal Carbides, J. Am. Chem. Soc. 136 (2014) 6385–6394. https://doi.org/10.1021/ja501520b.
[9] M. Khazaei, M. Arai, T. Sasaki, C.-Y. Chung, N.S. Venkataramanan, M. Estili, Y. Sakka, Y. Kawazoe, Novel Electronic and Magnetic Properties of Two-Dimensional Transition Metal Carbides and Nitrides, Advanced Functional Materials. 23 (2013) 2185–2192. https://doi.org/10.1002/adfm.201202502.
[10] D. Magne, V. Mauchamp, S. Célérier, P. Chartier, T. Cabioc'h, Site-projected electronic structure of two-dimensional Ti3C2 MXene: the role of the surface functionalization groups, Phys. Chem. Chem. Phys. 18 (2016) 30946–30953. https://doi.org/10.1039/C6CP05985F.
[11] M. Naguib, Y. Gogotsi, M.W. Barsoum, Mxenes: A New Family of Two-Dimensional Materials and Its Application As Electrodes for Li and Na-Ion Batteries, Meet. Abstr. MA2015-01 (2015) 849. https://doi.org/10.1149/MA2015-01/9/849.
[12] I. Persson, A. el Ghazaly, Q. Tao, J. Halim, S. Kota, V. Darakchieva, J. Palisaitis, M.W. Barsoum, J. Rosen, P.O.Å. Persson, Tailoring Structure, Composition, and Energy Storage Properties of MXenes from Selective Etching of In-Plane, Chemically Ordered MAX Phases, Small. 14 (2018) 1703676. https://doi.org/10.1002/smll.201703676.
[13] B. Anasori, Y. Xie, M. Beidaghi, J. Lu, B.C. Hosler, L. Hultman, P.R.C. Kent, Y. Gogotsi, M.W. Barsoum, Two-Dimensional, Ordered, Double Transition Metals Carbides (MXenes), ACS Nano. 9 (2015) 9507–9516. https://doi.org/10.1021/acsnano.5b03591.
[14] Q. Tao, M. Dahlqvist, J. Lu, S. Kota, R. Meshkian, J. Halim, J. Palisaitis, L. Hultman, M.W. Barsoum, P.O.Å. Persson, J. Rosen, Two-dimensional Mo1.33C MXene with divacancy ordering prepared from parent 3D laminate with in-plane chemical ordering, Nat Commun. 8 (2017) 14949. https://doi.org/10.1038/ncomms14949.
[15] S.K. Nemani, B. Zhang, B.C. Wyatt, Z.D. Hood, S. Manna, R. Khaledialidusti, W. Hong, M.G. Sternberg, S.K.R.S. Sankaranarayanan, B. Anasori, High-Entropy 2D Carbide MXenes: TiVNbMoC3 and TiVCrMoC3, ACS Nano. 15 (2021) 12815–12825. https://doi.org/10.1021/acsnano.1c02775.
[16] C. Chen, X. Xie, B. Anasori, A. Sarycheva, T. Makaryan, M. Zhao, P. Urbankowski, L. Miao, J. Jiang, Y. Gogotsi, MoS2-on-MXene Heterostructures as Highly Reversible Anode Materials for Lithium-Ion Batteries, Angewandte Chemie International Edition. 57 (2018) 1846–1850. https://doi.org/10.1002/anie.201710616.
[17] E.B. Deeva, A. Kurlov, P.M. Abdala, D. Lebedev, S.M. Kim, C.P. Gordon, A. Tsoukalou, A. Fedorov, C.R. Müller, In Situ XANES/XRD Study of the Structural Stability of Two-Dimensional Molybdenum Carbide Mo2CTx: Implications for the Catalytic Activity in the Water–Gas Shift Reaction, Chem. Mater. 31 (2019) 4505–4513. https://doi.org/10.1021/acs.chemmater.9b01105.
[18] H. Zhou, Z. Chen, E. Kountoupi, A. Tsoukalou, P.M. Abdala, P. Florian, A. Fedorov, C.R. Müller, Two-dimensional molybdenum carbide 2D-Mo2C as a superior catalyst for CO2 hydrogenation, Nat Commun. 12 (2021) 5510. https://doi.org/10.1038/s41467-021-25784-0.
[19] H. Zhou, Z. Chen, A.V. López, E.D. López, E. Lam, A. Tsoukalou, E. Willinger, D.A. Kuznetsov, D. Mance, A. Kierzkowska, F. Donat, P.M. Abdala, A. Comas-Vives, C. Copéret, A. Fedorov, C.R. Müller, Engineering the Cu/Mo2CTx (MXene) interface to drive CO2 hydrogenation to methanol, Nat Catal. 4 (2021) 860–871. https://doi.org/10.1038/s41929-021-00684-0.
[20] A. Kurlov, E.B. Deeva, P.M. Abdala, D. Lebedev, A. Tsoukalou, A. Comas-Vives, A. Fedorov, C.R. Müller, Exploiting two-dimensional morphology of molybdenum oxycarbide to enable efficient

catalytic dry reforming of methane, Nat Commun. 11 (2020) 4920. https://doi.org/10.1038/s41467-020-18721-0.
[21] R. Morales-Salvador, J.D. Gouveia, Á. Morales-García, F. Viñes, J.R.B. Gomes, F. Illas, Carbon Capture and Usage by MXenes, ACS Catal. 11 (2021) 11248–11255. https://doi.org/10.1021/acscatal.1c02663.
[22] Z.W. Seh, K.D. Fredrickson, B. Anasori, J. Kibsgaard, A.L. Strickler, M.R. Lukatskaya, Y. Gogotsi, T.F. Jaramillo, A. Vojvodic, Two-Dimensional Molybdenum Carbide (MXene) as an Efficient Electrocatalyst for Hydrogen Evolution, ACS Energy Lett. 1 (2016) 589–594. https://doi.org/10.1021/acsenergylett.6b00247.
[23] M. Benchakar, V. Natu, T.A. Elmelegy, M. Sokol, J. Snyder, C. Comminges, C. Morais, S. Célérier, A. Habrioux, M.W. Barsoum, On a Two-Dimensional MoS2/Mo2CTx Hydrogen Evolution Catalyst Obtained by the Topotactic Sulfurization of Mo2CTx MXene, J. Electrochem. Soc. 167 (2020) 124507. https://doi.org/10.1149/1945-7111/abad6e.
[24] D.A. Kuznetsov, Z. Chen, P.V. Kumar, A. Tsoukalou, A. Kierzkowska, P.M. Abdala, O.V. Safonova, A. Fedorov, C.R. Müller, Single Site Cobalt Substitution in 2D Molybdenum Carbide (MXene) Enhances Catalytic Activity in the Hydrogen Evolution Reaction, J. Am. Chem. Soc. 141 (2019) 17809–17816. https://doi.org/10.1021/jacs.9b08897.
[25] L. Loupias, R. Boulé, C. Morais, V. Mauchamp, N. Guignard, J. Rousseau, J. Pacaud, P. Chartier, M. Gaudon, C. Coutanceau, S. Célérier, A. Habrioux, Mo2CTx MXene supported nickel-iron alloy: an efficient and stable heterostructure to boost oxygen evolution reaction, 2D Mater. 10 (2023) 024005. https://doi.org/10.1088/2053-1583/acbfcb.
[26] R. Khaledialidusti, A.K. Mishra, A. Barnoush, Atomic defects in monolayer ordered double transition metal carbide (Mo2TiC2Tx) MXene and CO2 adsorption, J. Mater. Chem. C. 8 (2020) 4771–4779. https://doi.org/10.1039/C9TC06046D.
[27] M. Khazaei, M. Arai, T. Sasaki, M. Estili, Y. Sakka, Two-dimensional molybdenum carbides: potential thermoelectric materials of the MXene family, Phys. Chem. Chem. Phys. 16 (2014) 7841–7849. https://doi.org/10.1039/C4CP00467A.
[28] S. Jin, H. Jing, L. Wang, Q. Hu, A. Zhou, Construction and performance of CdS/MoO2@Mo2C-MXene photocatalyst for H2 production, J Adv Ceram. 11 (2022) 1431–1444. https://doi.org/10.1007/s40145-022-0621-3.
[29] D. Ontiveros, F. Viñes, C. Sousa, Bandgap engineering of MXene compounds for water splitting, J. Mater. Chem. A. 11 (2023) 13754–13764. https://doi.org/10.1039/D3TA01933K.
[30] A.D. Handoko, H. Chen, Y. Lum, Q. Zhang, B. Anasori, Z.W. Seh, Two-Dimensional Titanium and Molybdenum Carbide MXenes as Electrocatalysts for CO2 Reduction, iScience. 23 (2020) 101181. https://doi.org/10.1016/j.isci.2020.101181.
[31] R. Meshkian, L.-Å. Näslund, J. Halim, J. Lu, M.W. Barsoum, J. Rosen, Synthesis of two-dimensional molybdenum carbide, Mo2C, from the gallium based atomic laminate Mo2Ga2C, Scripta Materialia. 108 (2015) 147–150. https://doi.org/10.1016/j.scriptamat.2015.07.003.
[32] H. Kim, B. Anasori, Y. Gogotsi, H.N. Alshareef, Thermoelectric Properties of Two-Dimensional Molybdenum-Based MXenes, Chem. Mater. 29 (2017) 6472–6479. https://doi.org/10.1021/acs.chemmater.7b02056.
[33] J. Halim, K.M. Cook, P. Eklund, J. Rosen, M.W. Barsoum, XPS of cold pressed multilayered and freestanding delaminated 2D thin films of Mo2TiC2Tz and Mo2Ti2C3Tz (MXenes), Applied Surface Science. 494 (2019) 1138–1147. https://doi.org/10.1016/j.apsusc.2019.07.049.
[34] B. Anasori, C. Shi, E.J. Moon, Y. Xie, C.A. Voigt, P.R.C. Kent, S.J. May, S.J.L. Billinge, M.W. Barsoum, Y. Gogotsi, Control of electronic properties of 2D carbides (MXenes) by manipulating their transition metal layers, Nanoscale Horiz. 1 (2016) 227–234. https://doi.org/10.1039/C5NH00125K.
[35] A.D. Handoko, K.D. Fredrickson, B. Anasori, K.W. Convey, L.R. Johnson, Y. Gogotsi, A. Vojvodic, Z.W. Seh, Tuning the Basal Plane Functionalization of Two-Dimensional Metal Carbides (MXenes) To Control Hydrogen Evolution Activity, ACS Appl. Energy Mater. 1 (2018) 173–180. https://doi.org/10.1021/acsaem.7b00054.

[36] J. Halim, S. Kota, M.R. Lukatskaya, M. Naguib, M.-Q. Zhao, E.J. Moon, J. Pitock, J. Nanda, S.J. May, Y. Gogotsi, M.W. Barsoum, Synthesis and Characterization of 2D Molybdenum Carbide (MXene), Advanced Functional Materials. 26 (2016) 3118–3127. https://doi.org/10.1002/adfm.201505328.
[37] F. Kong, X. He, Q. Liu, X. Qi, Y. Zheng, R. Wang, Y. Bai, Effect of Ti3AlC2 precursor on the electrochemical properties of the resulting MXene Ti3C2 for Li-ion batteries, Ceramics International. 44 (2018) 11591–11596. https://doi.org/10.1016/j.ceramint.2018.03.223.
[38] C.E. Shuck, M. Han, K. Maleski, K. Hantanasirisakul, S.J. Kim, J. Choi, W.E.B. Reil, Y. Gogotsi, Effect of Ti3AlC2 MAX Phase on Structure and Properties of Resultant Ti3C2Tx MXene, ACS Appl. Nano Mater. 2 (2019) 3368–3376. https://doi.org/10.1021/acsanm.9b00286.
[39] C. Hu, C.-C. Lai, Q. Tao, J. Lu, J. Halim, L. Sun, J. Zhang, J. Yang, B. Anasori, J. Wang, Y. Sakka, L. Hultman, P. Eklund, J. Rosen, M.W. Barsoum, Mo2Ga2C: a new ternary nanolaminated carbide, Chem. Commun. 51 (2015) 6560–6563. https://doi.org/10.1039/C5CC00980D.
[40] X.H. Wang, Y.C. Zhou, Layered Machinable and Electrically Conductive Ti2AlC and Ti3AlC2 Ceramics: a Review, Journal of Materials Science & Technology. 26 (2010) 385–416. https://doi.org/10.1016/S1005-0302(10)60064-3.
[41] M.A. Hadi, M.S. Ali, New ordered MAX phase Mo2TiAlC2: Elastic and electronic properties from first-principles, Chinese Phys. B. 25 (2016) 107103. https://doi.org/10.1088/1674-1056/25/10/107103.
[42] B. Anasori, M. Dahlqvist, J. Halim, E.J. Moon, J. Lu, B.C. Hosler, E.N. Caspi, S.J. May, L. Hultman, P. Eklund, J. Rosén, M.W. Barsoum, Experimental and theoretical characterization of ordered MAX phases Mo2TiAlC2 and Mo2Ti2AlC3, Journal of Applied Physics. 118 (2015) 094304. https://doi.org/10.1063/1.4929640.
[43] C. Hu, C. Li, J. Halim, S. Kota, D.J. Tallman, M.W. Barsoum, On the Rapid Synthesis of the Ternary Mo2GaC, Journal of the American Ceramic Society. 98 (2015) 2713–2715. https://doi.org/10.1111/jace.13743.
[44] M. Khazaei, M. Arai, T. Sasaki, M. Estili, Y. Sakka, The effect of the interlayer element on the exfoliation of layered Mo2AC (A = Al, Si, P, Ga, Ge, As or In) MAX phases into two-dimensional Mo2C nanosheets, Science and Technology of Advanced Materials. 15 (2014) 014208. https://doi.org/10.1088/1468-6996/15/1/014208.
[45] M.A. Hadi, New ternary nanolaminated carbide Mo2Ga2C: A first-principles comparison with the MAX phase counterpart Mo2GaC, Computational Materials Science. 117 (2016) 422–427. https://doi.org/10.1016/j.commatsci.2016.02.018.
[46] X. Qi, W. Yin, S. Jin, A. Zhou, X. He, G. Song, Y. Zheng, Y. Bai, Density-functional-theory predictions of mechanical behaviour and thermal properties as well as experimental hardness of the Ga-bilayer Mo2Ga2C, J Adv Ceram. 11 (2022) 273–282. https://doi.org/10.1007/s40145-021-0531-9.
[47] X. Wang, C. Garnero, G. Rochard, D. Magne, S. Morisset, S. Hurand, P. Chartier, J. Rousseau, T. Cabioc'h, C. Coutanceau, V. Mauchamp, S. Célérier, A new etching environment (FeF3/HCl) for the synthesis of two-dimensional titanium carbide MXenes: a route towards selective reactivity vs. water, J. Mater. Chem. A. 5 (2017) 22012–22023. https://doi.org/10.1039/C7TA01082F.
[48] S. Célérier, S. Hurand, C. Garnero, S. Morisset, M. Benchakar, A. Habrioux, P. Chartier, V. Mauchamp, N. Findling, B. Lanson, E. Ferrage, Hydration of Ti3C2Tx MXene: An Interstratification Process with Major Implications on Physical Properties, Chem. Mater. 31 (2019) 454–461. https://doi.org/10.1021/acs.chemmater.8b03976.
[49] M. Ghidiu, M.R. Lukatskaya, M.-Q. Zhao, Y. Gogotsi, M.W. Barsoum, Conductive two-dimensional titanium carbide 'clay' with high volumetric capacitance, Nature. 516 (2014) 78–81. https://doi.org/10.1038/nature13970.
[50] M. Alhabeb, K. Maleski, B. Anasori, P. Lelyukh, L. Clark, S. Sin, Y. Gogotsi, Guidelines for Synthesis and Processing of Two-Dimensional Titanium Carbide (Ti3C2Tx MXene), Chem. Mater. 29 (2017) 7633–7644. https://doi.org/10.1021/acs.chemmater.7b02847.

[51] O. Mashtalir, M. Naguib, V.N. Mochalin, Y. Dall'Agnese, M. Heon, M.W. Barsoum, Y. Gogotsi, Intercalation and delamination of layered carbides and carbonitrides, Nature Communications. 4 (2013) 1716. https://doi.org/10.1038/ncomms2664.
[52] A. Sarycheva, Y. Gogotsi, Raman Spectroscopy Analysis of the Structure and Surface Chemistry of Ti3C2Tx MXene, Chem. Mater. 32 (2020) 3480–3488. https://doi.org/10.1021/acs.chemmater.0c00359.
[53] O. Chaix-Pluchery, A. Thore, S. Kota, J. Halim, C. Hu, J. Rosen, T. Ouisse, M.W. Barsoum, First-order Raman scattering in three-layered Mo-based ternaries: MoAlB, Mo2Ga2C and Mo2GaC, Journal of Raman Spectroscopy. 48 (2017) 631–638. https://doi.org/10.1002/jrs.5087.
[54] N.J. Lane, M. Naguib, V. Presser, G. Hug, L. Hultman, M.W. Barsoum, First-order Raman scattering of the MAX phases Ta4AlC3, Nb4AlC3, Ti4AlN3, and Ta2AlC, Journal of Raman Spectroscopy. 43 (2012) 954–958. https://doi.org/10.1002/jrs.3101.
[55] V. Presser, M. Naguib, L. Chaput, A. Togo, G. Hug, M.W. Barsoum, First-order Raman scattering of the MAX phases: Ti2AlN, Ti2AlC0.5N0.5, Ti2AlC, (Ti0.5V0.5)2AlC, V2AlC, Ti3AlC2, and Ti3GeC2, Journal of Raman Spectroscopy. 43 (2012) 168–172. https://doi.org/10.1002/jrs.3036.
[56] Y.F. Li, B. Xiao, L. Sun, X.Z. Wang, Y.M. Gao, Y.R. Wang, Phonon spectrum, IR and Raman modes, thermal expansion tensor and thermal physical properties of M2TiAlC2 (M=Cr, Mo, W), Computational Materials Science. 134 (2017) 67–83. https://doi.org/10.1016/j.commatsci.2017.03.036.
[57] L.-Å. Näslund, I. Persson, XPS spectra curve fittings of Ti3C2Tx based on first principles thinking, Applied Surface Science. 593 (2022) 153442. https://doi.org/10.1016/j.apsusc.2022.153442.
[58] V. Natu, M. Benchakar, C. Canaff, A. Habrioux, S. Célérier, M.W. Barsoum, A critical analysis of the X-ray photoelectron spectra of Ti3C2Tz MXenes, Matter. 4 (2021) 1224–1251. https://doi.org/10.1016/j.matt.2021.01.015.
[59] J. Zhang, K.A.S. Usman, M.A.N. Judicpa, D. Hegh, P.A. Lynch, J.M. Razal, Applications of X-Ray-Based Characterization in MXene Research, Small Methods. n/a (n.d.) 2201527. https://doi.org/10.1002/smtd.202201527.
[60] J. Halim, K.M. Cook, M. Naguib, P. Eklund, Y. Gogotsi, J. Rosen, M.W. Barsoum, X-ray photoelectron spectroscopy of select multi-layered transition metal carbides (MXenes), Applied Surface Science. 362 (2016) 406–417. https://doi.org/10.1016/j.apsusc.2015.11.089.
[61] I. Persson, L.-\AAke Näslund, J. Halim, M.W. Barsoum, V. Darakchieva, J. Palisaitis, J. Rosen, P.O. \AA Persson, On the organization and thermal behavior of functional groups on Ti3C2 MXene surfaces in vacuum, 2D Mater. 5 (2017) 015002. https://doi.org/10.1088/2053-1583/aa89cd.
[62] T. Schultz, N.C. Frey, K. Hantanasirisakul, S. Park, S.J. May, V.B. Shenoy, Y. Gogotsi, N. Koch, Surface Termination Dependent Work Function and Electronic Properties of Ti3C2Tx MXene, Chem. Mater. 31 (2019) 6590–6597. https://doi.org/10.1021/acs.chemmater.9b00414.
[63] J. Ma, W. Li, B.J. Morgan, J. Światowska, R. Baddour-Hadjean, M. Body, C. Legein, O.J. Borkiewicz, S. Leclerc, H. Groult, F. Lantelme, C. Laberty-Robert, D. Dambournet, Lithium Intercalation in Anatase Titanium Vacancies and the Role of Local Anionic Environment, Chemistry of Materials. 30 (2018) 3078–3089. https://doi.org/10.1021/acs.chemmater.8b00925.
[64] M. Ashton, K. Mathew, R.G. Hennig, S.B. Sinnott, Predicted Surface Composition and Thermodynamic Stability of MXenes in Solution, J. Phys. Chem. C. 120 (2016) 3550–3556. https://doi.org/10.1021/acs.jpcc.5b11887.
[65] K.A.S. Usman, J. Zhang, D.Y. Hegh, A.O. Rashed, D. Jiang, P.A. Lynch, P. Mota-Santiago, K.L. Jarvis, S. Qin, E.L. Prime, M. Naebe, L.C. Henderson, J.M. Razal, Sequentially Bridged Ti3C2Tx MXene Sheets for High Performance Applications, Advanced Materials Interfaces. 8 (2021) 2002043. https://doi.org/10.1002/admi.202002043.
[66] D.A. Kuznetsov, Z. Chen, P.M. Abdala, O.V. Safonova, A. Fedorov, C.R. Müller, Single-Atom-Substituted Mo2CTx:Fe-Layered Carbide for Selective Oxygen Reduction to Hydrogen Peroxide: Tracking the Evolution of the MXene Phase, J. Am. Chem. Soc. 143 (2021) 5771–5778. https://doi.org/10.1021/jacs.1c00504.